9 Material Screening

9.1 Introduction

The LZ sensitivity is assessed using a profile likelihood ratio (PLR) method, as described in Section 12. For material screening purposes, however, we evaluate conservative tolerable count rates by considering the residual events in a WIMP search region of about 0–20 detected photons (phd), equivalent to approximately 1.5 $\mathrm{keV_{ee}}$ to 6.5 $\mathrm{keV_{ee}}$ or 6 $\mathrm{keV_{nr}}$ to 30 $\mathrm{keV_{nr}}$. This energy window is functionally equivalent to the one employed in the full PLR method when considering the experiment's optimum sensitivity at about 40 GeV/c^2 WIMP mass. Events are considered within the 5.6 tonne fiducial mass, with vetoes from the liquid xenon (LXe) skin and outer detector (OD) applied, but before discrimination through S2/S1 and NR selection efficiency. In order for LZ to realize a sensitivity to a WIMP-nucleon cross section below 3×10^{-48} cm^2 within three years of data taking, the maximum tolerable electron recoil (ER) background from non-astrophysical sources is approximately 37×10^{-6} events/keV/kg/d (37 μdru). The nuclear recoil (NR) background must also be low, with ∼1 count in the exposure.

Although this represents an unprecedented low background rate for dark-matter detectors, it can be achieved through the use of several proven low-background assay techniques that have been successfully employed in recent rare-event searches for dark matter, as well as in neutrinoless double-beta decay and neutrino experiments [1–9]. The collaboration maintains significantly stricter goals for all the detector elements to reduce the risk of any one element violating the required levels: ∼37 μdru and an NR rate of ∼1 count in the exposure. In this section we frequently refer to the goals, which are between 1 - 10% of the levels specified as project requirements. The techniques LZ uses to monitor and control these backgrounds include:

- A comprehensive material-screening campaign to select components that satisfy stringent intrinsic radioactivity goals such that the single scatter rate within the fiducial volume and WIMP search energy range is less than 0.4 NR counts and below 1 μdru of ER background resulting from fixed contamination in the detector components;
- Direct measurements of radon emanation from construction materials for a maximum activity of 10 mBq throughout the liquid xenon. The goals for emanation are 1 mBq;
- Adherence to cleanliness protocols for control of airborne radioactivity and particulates to limit background at the level of that from materials to contact the LXe, contributing 10 mBq from radon emanation. This same level of surface contamination, in addition, contributes ER and NR backgrounds from the radioactive decays in the dust in the TPC and (α,n) reactions on the TPC components of 1 μdru ER and 0.4 NR counts, respectively. The goals for emanation from dust are <1 mBq with a corresponding reduction in ER and NR;
- Removal of radioactive elements such as Ar and Kr from the liquid xenon to limit their single scatter ER backgrounds in the WIMP search energy range to below 1 μdru.

Material screening is the primary route to controlling the ER and NR backgrounds resulting from radioactivity in the experiment. The measurement of radioactive isotopes in and on detector materials is required. These are primarily the γ-ray emitting isotopes ^{40}K; ^{137}Cs; and ^{60}Co, as well as ^{238}U, ^{235}U, ^{232}Th, and their

progeny. The U and Th chains are also responsible for neutron production following spontaneous fission and (α,n) reactions. Kr and Rn outgassing from materials into the Xe also results in ER backgrounds, and α-emitting Rn daughters can contribute to neutron backgrounds when deposited on certain materials.

Generally, radioactive contaminants in massive components or those closer to or within the central volume of Xe present more stringent cleanliness and radio-purity requirements. These include the PMTs, PMT bases and cables; the TPC components, including the PTFE sheets and support structures; and the Ti cryostat. Our screening campaign includes several mature techniques for the identification and characterization of radioactive species within these bulk detector materials, namely γ-ray spectroscopy with High Purity Germanium detectors (HPGe), Inductively-Coupled Plasma Mass Spectrometry (ICP-MS), Neutron Activation Analysis (NAA), and measurement of Rn emanation from components before their integration into LZ. These complementary techniques collectively produce a complete picture of the radiological contaminants. LZ has all of these available with sufficient sensitivity and throughput to meet the project goals, described in Section 9.3.

Detector components are matched with the appropriate assay technique depending on the material and requisite sensitivity, defined by Monte Carlo simulations described in Section 11.4. In some cases, the final detector material or components are assayed. When manufacturing or fabrication processes are complex, raw components as well as final components will be assayed to assist in maintaining purity through the manufacturing process and to assist in selecting those processes that do not introduce additional contamination.

Stringent constraints are also applied to "intrinsic" contamination of the Xe by radon, argon and krypton. The LZ Xe purification program will remove ^{85}Kr from the Xe down to the level of 0.015 ppt using chromatographic techniques (where concentration is for g/g here and throughput this section). The Xe purification program is detailed in Section 6. All components that come into contact with any Xe in the experiment, whether within the primary instrument or in the gas storage, circulation, or recovery pipework, are screened for fixed contaminants, Rn emanation, and Kr outgassing to ensure that the intrinsic background remains within defined limits. These emanation and outgassing measurements are performed in dedicated chambers built and operated by LZ institutions. Similarly, techniques to measure bulk contamination of materials with alpha-emitting radon progeny that are not readily identified using traditional HPGe, ICP-MS, or NAA have been developed by the collaboration. This is particularly important for the PTFE reflector panels within the TPC where prolonged exposure to radon-contaminated air during manufacture will result in the presence of alpha-emitting daughter of ^{210}Pb. The high cross section for (α,n) reactions on the fluorine in the PTFE will result in neutron emission, setting stringent constraints on ^{210}Pb content in the bulk material.

The results of screening measurements are entered into an LZ materials database and build on the existing LUX screening campaign data [10]. The database collates assay results from materials selected for use and identifies the components that contain them. These are referenced to results from Monte Carlo simulations that detail the background from the components in LZ. The contributions from several other sources are included in the database, where each contributes no more than materials radioactivity ER and NR goals. The first is the contribution from dust and radon-daughter plate-out on components, especially during component transport, storage, and assembly. This is controlled through use of dedicated cleanrooms available to the project at SURF (especially the radon-reduced Surface Assembly Laboratory), active monitoring of the environment for radon, and following established cleanliness, handling, and storage procedures. Selected lightweight plastics and rubbers with low radon diffusion coefficients are used to enclose materials in transit and during temporary storage. Coupons and witness plates are used for measurements of surface contamination with high sensitivity alpha-screening devices and cameras. The second contribution comes from cosmogenic activation of components before they are moved underground, such as ^{46}Sc production from Ti activation or ^{127}Xe and radioactivity from the laboratory environment. While contribution to the background from local radioactivity and potential activation products including radioactive isotopes of Xe are assessed with a number of simulation toolkits, data from the LUX experiment in particular is able to provide considerable input to reduce the systematic uncertainty for such calculations.

Although the sensitivity goals for LZ require unparalleled low-background contamination control for dark matter experiments and consequent severe constraints on material contamination, the screening campaign outlined here builds on the demonstrated substantial experience of the collaboration and established procedures or techniques employed by rare-event searches for background mitigation to meet these challenges with confidence. The LZ collaboration has accomplished important steps in developing necessary infrastructure for our assay and cleanliness program, and in identifying appropriately low-activity materials for the five most critical detector components or materials including Ti for the cryostat, PTFE used in several locations in the inner TPC, PMT base materials, PMT raw materials, and stainless steel for large mass support structures. In the following subsections we define the goals and requirements for our screening program, present the details of assays associated with the major components together with our collected data for all materials, present the impact of the background sources in LZ as determined through Monte Carlo simulations, and summarize the techniques and resources available to the project to meet our assay and cleanliness requirements on schedule.

9.2 Goals, Requirements and Estimates

The LZSim Monte Carlo simulation package, described in detail in Section 11.4, has been constructed to model the experiment and inform the design, determine optimal performance parameters, and define tolerable rates from background sources. Developed using the GEANT4 toolkit [11], the framework inherits from, and closely follows, the successful implementation of the LUX model [12], with evolving design of all parts of the experiment, including the inner detector, Xe skin, cryostat, and the OD, reflected in appropriate changes to the model geometry.

Simulations are performed to assess the contribution from all expected background sources, including intrinsic radioactivity in the Xe, emission from every component in the experiment, as well as estimates of neutrino interactions. This extends to subcomponents, with the model accurately representing the physical distribution of contaminants, particularly since (α,n) neutron yields vary by many orders of magnitude depending on the primary constituents of the materials containing the alpha-emitting uranium and thorium and decay products. Similarly, the physical distribution of γ-ray, alpha, and beta particle emitters are modeled, as electrons created by these may produce detectable photons through Cherenkov and Bremsstrahlung processes, particularly in quartz or plastics close to or in contact with Xe. Evaluations of material radioactivity include contributions from spontaneous fission of heavy nuclei. Spontaneous fission of ^{238}U, ^{235}U, ^{234}U, ^{231}Pa, ^{230}Th, or ^{232}Th, present in the U and Th decay chains generates multiple prompt and delayed neutrons and γ-rays per decay. LZSim models these products with accurate energy, multiplicity, timing, and angular distributions. The single scatter identification capability in the TPC coupled to the high vetoing efficiency of the Xe skin and OD systems allow >99.99 % rejection of all spontaneous fission events, and effective removal from our background models. The performance of the veto skin and OD veto systems are presented in Section 3.7 and Chapter 4, respectively. Events in the TPC with associated energy depositions identified in the Xe skin or OD with signal equivalent to approximately equal to or more than 100 keV in Xe skin and 200 keV in OD are rejected.

All energy depositions from interactions in the Xe and OD are recorded in LZSim. Where necessary, optical tracking is performed following scintillation and ionization generation implemented using NEST [13]. LZSim models photon hit patterns and timing to mimic S1 and S2 signal generation in LZ, and allows for accurate studies of rare mechanisms that might produce backgrounds such as MSSI (multiple-scintillation single-ionization) events or background pile-up. Such detailed characterization and quantification of all background sources and their impacts are necessary to assign confidence to expected background event rates, their spectra, and their physical distribution in the detector. As a discovery instrument, the expected background in

LZ must be well understood and quantified before significance can be ascribed to observation of any potential signal and WIMP discovery.

Version controlled release management of LZSim includes validation of materials and geometries against CAD drawings, physics lists implementation and detector response using pre-defined macros, and impact tests from radio-activity released from major components as well as from specific benchmark locations distributed throughout the detector volumes. Details of LZSim and the simulations are given in Section 11.4.

With the exception of astrophysical neutrinos discussed in Section 2.2, the major sources of background in LZ will be radioactivity from construction materials surrounding the central fiducial volume, and radon daughters and krypton distributed throughout the xenon. The goal for the maximum unvetoed differential single-scatter ER rate from each of these non-astrophysical sources after cuts in the WIMP search energy range has been set to about 1 µdru. This is approximately 10 % of that expected from irreducible pp solar neutrinos deduced from our Monte Carlo simulations of the detector. Similarly, an upper limit of 0.4 unvetoed WIMP-like single-scatter NRs due to neutron emission from material radioactivity is the goal for a 1,000-day exposure, reduced to 0.2 after a 50 % NR efficiency is applied. Goals for maintaining cleanliness throughout the experiment construction, for parts manufacture, transport, storage, assembly and integration, allow for contribution to ER and NR background equivalent to that from materials. Table 9.2.7 presents the estimate of the backgrounds in the experiment. Material assay results in hand and achieved by similar collaborations form the input for material activity, and these meet project goals. Values for radon emanation are based on conservative estimates, as described in Section 9.5, that match our requirements, but are currently estimated to exceed our goals. As we assay our materials we anticipate a reduction from this contribution to Table 9.2.7. The project requirements are discussed in Section 12, where the sensitivity of LZ to WIMP dark matter is presented. The LZ collaboration maintains more aggressive goals for its radioactive backgrounds for several reasons. The first is to provide contingency for measured radio-content in materials and for intrinsic contributions, invoking safety factors that mitigate large variations in expected and final radioactivity. Second, the goals facilitate simplified analyses, with total material and intrinsic background contributions sub-dominant to the ER backgrounds from astrophysical neutrinos that will be uniformly distributed across the active volume. Finally, our goals enhance physics capability beyond the primary WIMP search, as described in Section 2, particularly for neutrino interactions, neutrinoless double-beta decay, and alternative dark matter models including axion-like particles (ALPs).

Acceptance of screened materials for use in LZ depends on the Monte Carlo simulations and the overall radioactive background budget. When a component is identified as required in LZ, it is incorporated into the LZSim model and a preliminary estimate of maximum tolerable activity from that component is calculated. This requirement necessarily depends on activity from other components and the overall budget, and initial inputs to LZSim for detector-related backgrounds are based on measured values, or from screening results from previous experiments. Initially the background budget is evenly divided among the major components, such that if there are ten components, the allowable background for each component is assigned 1/10 of the allowable contamination. The maximum tolerable activity for the new component, including contingency for dominant materials such as the PMTs, is then translated to a required screening sensitivity for radio-assaying a material sample. This in turn informs the screening technique and facility that will be employed for the assay. Screening results are then fed back into LZSim to produce an accurate assessment of ER and NR background and overall impact. The acceptance of the component depends on whether it meets requirements, or if it can be accommodated given related constraints and achieved radio-purity in other components and materials. In some cases, and as is justified by our assay experience, we may employ sampling of complete components. As the materials are assayed, this screening provides "as-built" input for the LZ background model.

The ER and NR background calculations take into account radioactivity from all the components. Requirements on different materials and components vary, with their impact depending on material and position in the experiment. The simulations inform the necessity for screening U and Th in materials at the order of

tens of ppt levels, tens to hundreds of ppb for K, and 0.05 mBq/kg for ^{60}Co. Sensitivity at 10 mBq/kg to ^{210}Pb in bulk materials is required. Radon emanation systems are required to meet sensitivity to ^{222}Rn at the level of 0.3 mBq from materials. Cleanliness-maintenance procedures that will be applied to all materials to guarantee adequate background control and accurate modeling set requirements on maximum dust or radon exposure, calculated taking into account assembly and integration duration. We require less than a 10 mBq contribution to ER background from dust, conservatively equivalent to less than 1 g of dust in total on all wetted surfaces. We require a maximum ^{210}Pb activity from radon progeny on surfaces of 10 mBq/m^2, reduced to 0.5 mBq/m^2 for the inner surfaces of the TPC reflectors.

Materials of sufficient radio-purity have been successfully deployed in rare-event search experiments and will be procured and incorporated in the LZ project following sample/component measurements with available technology and facilities that incorporate screening, cleanliness maintenance, and outputs from the completed R&D program. These measurements and procedures are well on the way to reliably identify clean materials and maintain their purity throughout the chain, from fabrication to installation and operation. The assaying program to achieve these minimum limits and estimates adopted are detailed below.

9.2.1 Materials Table

Table 9.2.1 presents the justification for the assumed values of ^{238}U, ^{232}Th, ^{60}Co, and ^{40}K content used as initial input to LZSim for the major components. Throughout this document, we refer to early and late values for ^{238}U and ^{232}Th. In the case of ^{238}U, we define the early part of the chain ($^{238}U_e$) as containing any isotopes above ^{226}Ra since chemical processes may induce a break of secular equilibrium at this point and it will take many years to be restored. The late part of the chain ($^{238}U_l$) is counted from ^{226}Ra and below. In practice, standard HPGe detectors are not sensitive to the low-energy γ-ray lines from ^{210}Pb at the bottom of the chain but the BEGe and well-type detectors available to LZ are (see Section 9.4.1.2). We populate the table with values for ^{210}Pb where appropriate for our materials and assays. For the ^{232}Th chain, we define the early part of the chain ($^{232}Th_e$) as coming from isotopes above ^{224}Ra and the late part of the chain ($^{232}Th_l$) as coming from isotopes below as chemical processes may, again, break the secular equilibrium. The relatively long half-life of ^{228}Ra (5.7 y) means that, for example, with 100 % removal of Ra isotopes it would take ~50 y for ^{228}Ra and ^{224}Ra to re-equilibrate. LZ and LUX assays are maintained in our dedicated database but for those items which we are yet to screen, XENON100 assays are taken from [14]; EXO-200 from [1]; XENON1T [15]; MAJORANA, GERDA, and SuperNEMO by private communication or conference presentations; SNO from [16].

Our assay campaign has made good progress in measuring the main contributors to the experiment's ER and NR backgrounds and those that represent challenging requirements. LZ has performed over 250 material assays from April 2015 to October 2016, and have already identified five critical components or materials that collectively account for 60 % of the NR and 50 % of ER background from intrinsic material radioactivity in LZ. These are the Ti used for the cryostat, field shaping rings, and PMT support structures; PMTs including all PMT raw materials; PMT base components; stainless steel for OD supports; and PTFE. All these materials satisfy the LZ goals that are well below the project requirements. Below we summarize the assay campaigns and results from these components and materials.

Titanium: The two cryostat vessels and flanges will be constructed with CP-1 grade titanium. The selected material has measured ^{238}U and ^{232}Th chain activities of <0.09 mBq/kg and 0.23 mBq/kg, respectively, representing the lowest reported to-date worldwide and substantially below the LZ goals. Two billets of Ti from the same production lot have been assayed and material procured to provide the raw material for all Ti components. The field-shaping rings, constructed from 260 kg of Ti, and the PMT support structures, constructed from 104 kg of Ti, will use the same raw material as the cryostat.

Table 9.2.1: Materials in the LZ design listed with radioactivity mBq/kg as determined by direct assay data from the LZ screening program, and from other published experimental results. Reference values are from LZ[1], EXO-200[2], XENON100[3], SuperNEMO[4], SNO[5] and GERDA[6]. The activities shown represent error weighted averaged values for γ-ray detection or 68 % C.L. upper limits (italicized).

Material	$^{238}U_e$	$^{238}U_l$	$^{232}Th_e$	$^{232}Th_l$	^{60}Co	^{40}K	^{210}Pb
Values in (mBq/kg)							
General Materials							
Titanium[1]	*1.60*	*0.09*	0.28	0.23	*0.02*	*0.54*	-
PTFE[2]	*0.02*	*0.02*	*0.03*	*0.03*	-	*0.12*	-
PEEK[1]	17.0	16.6	16.1	8.50	*0.52*	47.8	-
LED[1]	2000	*100.0*	*200*	*100.0*	-	*1000*	-
Copper[1]	*1.30*	*1.20*	*14.5*	*1.70*	*0.40*	*7.00*	-
Cable (RG174)[3]	29.8	1.47	3.31	3.15	0.65	33.1	-
Stainless Steel[1]	1.20	0.27	0.33	0.49	1.60	0.40	-
Epoxy[2]	0.55	0.55	0.10	0.10	-	0.63	-
Viton O-ring[1]	2630	2490	220	220	10.0	2150	-
Tyvek[4]	6.00	6.00	2.20	2.20	-	5100	-
HDPE[5]	5.96	0.37	0.63	0.62	-	3.40	-
Rubber O-ring[2]	124	124	41.0	41.0	-	24.5	-
Mini-HV cable[1]	40.0	2.10	1.50	1.30	-	0.17	-
Liquid Scintillator							
LAB[1]	0.00005	0.00005	0.00003	0.00003	-	0.00001	-
$GdCl_3$.$6H_2O$ [1]	1.24	1.24	0.41	0.41	-	0.0006	-
PPO[1]	*1.85*	*1.85*	*2.60*	*2.60*	-	*0.0008*	-
TMHA[1]	*0.25*	*0.25*	*0.29*	*0.29*	-	*0.0003*	-
bis-MSB[1]	*2.60*	*2.60*	*0.78*	*0.78*	-	*0.0009*	-
Outer Detector							
Glass bulb[1]	1507	1507	1065	1065	-	3900	-
LS Tanks[2,5]	*0.01*	*0.01*	*0.005*	*0.005*	-	*0.07*	-
Displacement foam[1]	20.0	57.0	*2.60*	*9.00*	*6.00*	*80.0*	-
PMT Base Materials							
Resistors (4.99M)[1]	965	284	240	172	*18.0*	3249	35475
Capacitors[1]	4540	11715	4035	4035	*10.0*	350	11590
Cirlex Board[1]	23.9	19.1	3.19	3.19	*0.63*	*15.1*	25.5
Solder[1]	*58.2*	*11.8*	*10.7*	*10.7*	*2.24*	*31.8*	-
Receptacles: PMT pins[1]	1178	*7.00*	22.0	15.0	-	110	22393
Receptacles: Signal/HV[1]	833	7.50	13.2	15.4	-	77.3	21171
Receptacles: Ground[1]	568	20.5	16.7	8.20	-	*19.0*	29112
Resistors (7.5M)[1]	1097	389	106	106	*16.3*	3082	41600
Resistors (10.0M)[1]	2420	414	226	226	*11.6*	987	21613
Resistors (2.49M)[1]	1787	571	645	150	*65.0*	7069	52702
Resistors (100k)[1]	3460	1036	510	144	*169*	6118	97516

(continued on next page)

Material	$^{238}U_e$	$^{238}U_l$	$^{232}Th_e$	$^{232}Th_l$	^{60}Co	^{40}K	^{210}Pb
Values in (mBq/kg)							
Resistors (50)[1]	3430	670	314	264	*29.0*	5425	61140
Receptacles: Spring[1]	4758	38.0	50.0	50.0	*7.00*	131	1364
R11410 PMTs							
Metal Bulb[1]	*17.9*	*0.90*	*1.67*	*1.28*	-	*6.41*	-
Dynode[1]	*216*	*2.02*	*4.10*	*3.40*	4.00	*4.60*	-
Shield Plate[1]	*77.0*	*3.10*	*5.00*	*3.20*	4.60	*6.00*	-
Faceplate[1]	*11.0*	*0.67*	*1.00*	*0.80*	-	*4.00*	-
Insulator plate[1]	*20.9*	*1.05*	*1.63*	*1.16*	-	*6.28*	-
Electrode Disk[1]	*203*	9.50	*4.30*	14.0	8.50	*9.60*	-
Faceplate Flange[1]	*162*	*2.75*	*3.80*	*4.20*	12.5	*14.4*	-
Ceramic Stem[1]	105	20.0	12.9	9.60	-	110	5.60
Ceramic Stem Flange[1]	*198*	*0.63*	*2.32*	*0.84*	12.0	*3.30*	-
Aluminium Ring[1]	*62.0*	*1.23*	2.33	*0.94*	*0.34*	*8.50*	-
Getter[1]	*2508*	*39.0*	*133*	*102*	*9.40*	*173*	-
Stem Coating[1]	*22.0*	178	*9.00*	7.50	-	61.0	*539*
R8520 Skin PMTs							
Metal Package[3]	19.0	19.0	*13.0*	*13.0*	40.0	90.0	-
Glass in Stem[3]	970	970	340	340	*10.0*	2300	-
Spacer[3]	780	780	260	260	*12.0*	800	-
Seal[3]	17.0	17.0	370	370	*27.0*	5.00	-
Electrodes[3]	19.0	19.0	18.0	18.0	12.0	0.15	-
Window[3]	*0.50*	*0.50*	*1.80*	*1.80*	*0.10*	18.0	-
TPC Items							
Loop Antenna Wire[2]	0.20	0.20	0.12	0.12	-	*1.86*	-
Thermometers[1]	4038	3433	1439	1042	*6.6*	156416	1364
Acoustic Sensor PVDF[1]	1710	595	2179	1951	-	1389	-
Field Shaping Resistor[1]	5679	1.73	0.57	0.57	-	0.19	-
HV Conduits							
Tivar[1]	*6.20*	22.2	*1.22*	*1.22*	-	*9.30*	-
Delrin[4]	*4.00*	*0.70*	*0.18*	*0.18*	*0.30*	18.0	-
Cryostat Insulation							
SI Aluminium[6]	1.13	1.13	0.37	0.37	-	25.5	-
SI PTFE[6]	0.34	0.34	0.75	0.75	-	38.0	-
Foam-insulation[1]	57.0	57.0	9.00	9.00	*6.00*	*80.0*	-
Helicoil[2]	*2.40*	*2.40*	*1.30*	*1.30*	41.0	*13.5*	-

A long campaign in assaying titanium from various sources and states of processing has been underway for a couple years, including investigation of alternative options such as stainless steel. The cryostat material assays have primarily been carried out by the Berkeley Low Background Facility using its surface screening detectors at LBNL and the underground HPGe system MAEVE both before and after its relocation from the

Oroville Dam to the 4850L of SURF (see Section 9.4.1.1). Moreover, there is consistency in multiple assays of similar geometries with this HPGe counter which was also used to assay titanium samples ultimately selected for use in LUX. Dozens of titanium and stainless steel samples were assayed for the LZ experiment. As seen in Figure 9.2.1 a wide range of radioactivity values have been covered and that, in general, titanium has been more consistently clean as compared to stainless steel, which varies in both the natural radionuclides as well as ^{60}Co.

The selected titanium sample from TIMET, Heat Number (HN) 3469 was initially screened at the Berkeley Low Background Facility using MAEVE in May of 2015. This initial sample consisted of 10.1 kg of plates selected from the top portion of the single slab that comprised this heat (HN3460-T). A second sample from this slab, taken from the middle (HN3469-M), was acquired and assayed in September of 2015. Both samples of this titanium stock were found to be consistent with one another with their contained radioactivity. The samples were analyzed using a GEANT4 model of the MAEVE detector with an exact sample geometry of the titanium placed around the detector on four sides and the top to simulate detection efficiency of γ-rays in the regions of interest for the detector. The simulation was first compared to calibrated samples of known activity to benchmark the detector geometry, then modeled with the titanium geometry. As a check, the titanium sample was also directly compared to a calibration sample in a similar geometry, which agreed well with the analysis performed with a simulated efficiency.

In both of the samples, each counted for approximately three weeks, the early uranium chain was non-detectable or barely detectable within the limited abilities of HPGe detectors to assay this portion of the decay chain via γ-ray spectroscopy. The late portion of the chain (at ^{226}Ra and below) however, is quite accessible via γ-ray spectroscopy due to both the branching ratio and detection efficiency for γ-rays emitted during the decay of constituent isotopes, registered no detectable activity above background down to the few ppt level. The late uranium value is based upon the 609 keV peak from ^{214}Bi and is consistent when compared to upper limits from other useful peaks in the late uranium chain (such as 295, 352, and 1,764 keV). Both samples had detectable levels of the thorium series in both the early and late portions of the chain which implied equilibrium in both samples. The late series measurement is based upon the 238 keV γ-ray from ^{212}Pb, which is the strongest peak based upon the product of the detection efficiency of that γ-ray line and its branching ratio in the thorium chain for assay with MAEVE. The contributions of the uranium, thorium, and potassium concentrations varies across the chains and their corresponding decays. The assays are summarized in Table 9.2.2. The late uranium chain in the titanium cryostat, for example, is a larger overall source of NR backgrounds within the detector than the early uranium chain because there is a rapid succession of several high energy alpha decays which induce (α,n) reactions. These various contributions from the chains towards the detector background are totaled and accounted for within Figure 9.2.1.

In terms of cosmogenic activation there were several isotopes of scandium present, most of which are the result of cosmic ray-induced reactions with the several stable isotopes of titanium. Detected in the sample was ^{46}Sc (889, 1,120 keV); as well as small amounts of ^{47}Sc (159 keV), ^{48}Sc (983, 1,037, 1,312 keV), and ^{44,44m}Sc (271, 1,157 keV). None of the scandium isotopes are a cause of concern as they are all short-lived, the longest of which is ^{46}Sc with a half live of 84 d is listed in Table 9.2.2. The ^{47}Sc, ^{48}Sc, and ^{44,44m}Sc activities were not listed as they have short half lives of a few days or less so essentially disappear over the course of the measurement. The reported value for ^{46}Sc was decay corrected to the start of counting for each of the samples. All limits are one sigma upper limits and uncertainties are statistical only. A conservative systematic uncertainty of up to 10 % should also be assumed. The assays have being confirmed by ICP-MS and with additional direct counting assays with the Chaloner detector at Boulby.

R11410 PMTs: The activity for early production models of the 3-inch R11410 PMTs has been measured by the LZ collaboration [17]. Multiple batches of PMTs (25 total) were assayed in groups of five. The raw material used to produce the experiment's PMTs were also assayed. The component materials used to produce the final LZ PMTs have now been assessed for radio-purity. The results are presented in Table 9.2.3,

Table 9.2.2: Results from γ-ray spectroscopy of TIMET titanium HN3469 for both Top and Middle samples. All limits are one sigma upper limits and uncertainties are statistical only. A systematic uncertainty of up to 10 % should also be assumed. The results are shown below as activities in the ^{238}U, ^{232}Th, and ^{40}K chains — all in units of mBq/kg. Results were obtained with the MAEVE detector and confirmed with ICP-MS and the Chaloner detector.

	Top	Middle
date	5-2015	9-2015
sample mass	10.07 kg	8.58 kg
livetime	23.9 d	20.8 d
$^{238}U_e$	< 1.6	2.9(15)
$^{238}U_l$	< 0.09	< 0.10
$^{232}Th_e$	0.28(3)	< 0.20
$^{232}Th_l$	0.23(2)	0.25(2)
^{40}K	< 0.54	< 0.68
^{60}Co	< 0.02	< 0.03
^{46}Sc	2.0(1)	2.7(1)

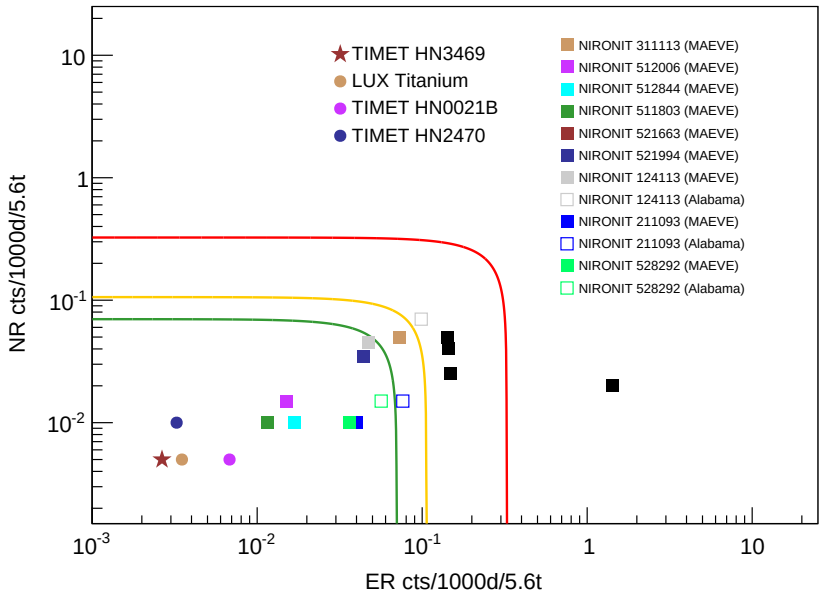

Figure 9.2.1: The plot shows the background counts resulting from LZ's Ti (TIMET) and stainless steel (NIRONIT) samples from the LXe cryostat in the 1,000 d-exposure with a 5.6 tonne-fiducial volume and after all the veto systems are applied, for ER events within 1.5 keV$_{ee}$ to 6.5 keV$_{ee}$, with 99.5 % rejection, and within 6 keV$_{nr}$ to 30 keV$_{nr}$, and 50 % acceptance, for NR events. The red curve corresponds to the sum of 10 % of the pp solar neutrinos background for ERs and of 0.2 NR events. The yellow curve is for the sum of 5 % of the pp neutrino background and 0.05 NR events. The green curve corresponds to the sum of 3.3 % of the pp neutron background and 0.03 NR events, the requirement for the LZ cryostat. The Ti identified by the assay program, indicated by the star, is well below requirements of LZ.

and are generally consistent with results from the XENON1T collaboration (albeit using 68 % rather than 90 % CL upper limits) following a similar campaign of screening of their R11410 PMTs and constituent materials [15]. The LZ assays of PMT materials have been performed with γ-ray spectroscopy principally with the SOLO detector and coordinated by the Brown University group, with the MAEVE detector at SURF and Chaloner detector at Boulby providing additional throughput and low energy sensitivity, particularly for early U chain content. Details of these detectors are given in Section 9.4.1. The materials have been returned to Hamamatsu and PMT production is underway. Screening of tubes that will be installed in LZ has begun at Boulby using the Chaloner and Lunehead detectors and will continue through 2017 when the screening will also be supported by the BHUC detectors.

PMT Bases: The activity of the components used to produce the bases for the R11410 TPC and R8520 Xe skin PMTs have been assayed at Boulby, principally with the Chaloner detector. These items include the resistors, capacitors, connectors and substrate material. We have also performed assays to measure ^{210}Pb content in these materials, exploiting the capability of Boulby's Lumpsey detector (described in Section 9.4.1.2). This contamination is challenging to assay and usually overlooked, despite it being present in large quantity in components such as resistors and capacitors, with the potential to contribute significantly to neutron production. The ^{210}Pb is accounted for in our background model. The radioactivity of the base components meet LZ goals and are presented for the TPC PMTs in Table 9.2.4, and for the Xe skin in Table 9.2.5.

Table 9.2.3: Intrinsic radioactivity of the component materials which will be used in the manufacture of the R11410-20 PMTs to be used in the LZ experiment. All values are presented in mBq/kg of material. Measurements are performed using the SOLO detector [1], MAEVE [2], and Chaloner [3]. Upper limits are italicized

Values in (mBq/kg)									
Material	Mass screened (g)	Mass /PMT (g)	$^{238}U_e$	$^{238}U_l$	$^{232}Th_e$	$^{232}Th_l$	^{60}Co	^{40}K	^{210}Pb
Metal Bulb[2]	506	78	*17.9*	*0.90*	*1.67*	*1.28*	-	*6.41*	-
Dynode[1]	530	7.2	*216*	*2.02*	*4.10*	*3.40*	4.00	*4.60*	-
Shield Plate[1]	519	4	*77.0*	*3.10*	*5.00*	*3.20*	4.60	*6.00*	-
Faceplate[2]	1168	30	*11.0*	*0.67*	*1.00*	*0.80*	-	*4.00*	-
Insulator plate[2]	838	8.6	*20.9*	*1.05*	*1.63*	*1.16*	-	*6.28*	-
Electrode Disk[1]	517	9.9	*203*	9.50	*4.30*	14.0	8.50	*9.60*	-
Faceplate Flange[1]	532	18	*162*	*2.75*	*3.80*	*4.20*	12.5	*14.4*	-
Ceramic Stem[1,3]	757.5	15.7	105	20.0	12.9	9.60	-	110	5.60
Ceramic Stem Flange[1]	1568	14	*198*	*0.63*	*2.32*	*0.84*	12.0	*3.30*	-
Aluminium Ring[1]	506	0.6	*62.0*	*1.23*	2.33	*0.94*	*0.34*	*8.50*	-
Getter[1]	7	0.07	*2508*	*39.0*	*133*	*102*	*9.40*	*173*	-
Stem Coating	100	0.00012	*22.0*	178	*9.00*	7.50	-	61.0	*539*
Mass Weighted Ave		**186.1**	***71.6***	***3.20***	***3.12***	***2.99***	***2.82***	***15.4***	***0.47***
Total (mBq/PMT)		**186.1**	***13.3***	***0.60***	***0.58***	***0.56***	***0.53***	***2.87***	***0.09***

Table 9.2.4: Assay results from 3-inch R11410 PMT base component materials. All values are presented in mBq/base.

Values in (μBq/base)									
Material		**Mass per base (mg)**	**$^{238}U_e$**	**$^{238}U_l$**	**$^{232}Th_e$**	**$^{232}Th_l$**	**^{60}Co**	**^{40}K**	**^{210}Pb**
Resistors	4.99M	34.4	32.8	14.1	7.3	5.9	*0.6*	130	1290
	7.5M	14.1	15.3	5.4	1.5	1.5	*0.3*	43.2	584
	10.0M	12.9	31.5	5.3	2.9	2.9	*0.2*	12.8	280
	50R	4.3	12.9	2.9	1.4	1.1	*0.1*	23.5	265
Capacitors	10nF	24.5	111	286	98.5	98.5	*0.1*	8.5	283
Receptacles	PMT Pins	1170	775	*6.5*	25.8	12.8	*6.0*	129.0	26200
	Signal/HV	156	103.4	*0.9*	3.4	1.7	*0.8*	17.2	3495
	Ground	244.2	103.4	*0.9*	2.9	1.7	*0.8*	15.2	5780
Base	Cirlex	3300	94.8	66.8	13.8	13.8	*2.0*	*40.5*	56.8
Solder	Pb Free	180	*10.5*	*2.1*	*1.9*	*1.9*	*0.4*	*5.7*	*63.0*
Total		**5140**	***1291***	***390***	***159***	***143***	***11***	***426***	***38300***

Table 9.2.5: Assay results from 1-inch R8520 skin component materials. All values are presented in mBq/base.

Values in (μBq/base)									
Material		**Mass per base (mg)**	**$^{238}U_e$**	**$^{238}U_l$**	**$^{232}Th_e$**	**$^{232}Th_l$**	**^{60}Co**	**^{40}K**	**^{210}Pb**
Resistors	4.99M	34.4	32.8	14.1	7.3	7.3	*0.6*	130	1292
	7.5M	4.7	5.1	1.8	0.5	0.5	*0.1*	14.4	195
	10.0M	4.3	10.5	1.8	0.1	0.1	*0.1*	4.28	93.4
	2.49M	8.4	15	4.8	1.2	1.2	*0.5*	59.4	443
	100k	3.6	12.3	3.7	0.5	0.5	*0.6*	21.8	347
Capacitors	10nF	14.7	66.3	171	59.1	59.1	*0.2*	5.1	170
Receptacles	Signal/HV	156	103	0.9	1.7	1.7	*0.8*	17.2	3495
	Ground	244	103	0.9	1.7	1.7	*0.8*	15.2	5780
Base	Cirlex	1400	40.2	28.3	5.8	5.8	*0.8*	*17.2*	24.1
Solder	Pb Free	250	*10.5*	*2.1*	*1.9*	*1.9*	*0.4*	*5.7*	*63.0*
Total		**2120**	***400***	***230***	***81***	***81***	***5***	***291***	***11900***

Stainless Steel: The base of the OD support stand and water PMT stands total some 770 kg of material and are constructed from stainless steel. The assay values are taken from the LZ determination of NIRONIT raw material using the MAEVE detector. These samples were identified as part of our R&D campaign to select and procure sufficiently low background material for the detector cryostat. Though there is large variation across the sample activities, activities as low as <1.60 mBq/kg ^{238}U and 0.23 mBq/kg ^{232}Th have been realized. Goals for OD support radioactivity are easily met by all of the samples assayed. In addition to the OD supports stainless steel will be used for several internal structures such as grid supports and pipework. Several NIRONIT samples meet the radioactivity goals and all meet the requirements for these components. Candidate materials for procurement and the materials used for the final fabrication will be assayed.

PTFE: The LZ collaboration has assayed four samples of PTFE in September 2015 using NAA at the MIT Research Reactor with surface γ-ray counters at Alabama. The NAA technique is described in Section 9.4.3. The samples were prepared at Alabama together with NIST certified fly ash used to calibrate the neutron flux, and measured in port 2PH1 with 5.5 MW of thermal reactor power. The samples include material from Flontech and DuPont, where the latter is the supplier used by the EXO experiment, employing sintering techniques developed with Applied Plastics Technology Inc. (APT) in Bristol, Rhode Island. The assayed contamination levels are presented in Table 9.2.6. While these are slightly higher than those obtained by EXO, they satisfy the radioactive contamination goals of LZ.

LZ has developed assay capability to determine the ^{210}Pb content of the bulk materials used to fabricate the PTFE. The Lumpsey detector at Boulby, described in Section 9.4.1.2, has sensitivity meeting the requirement of 10 mBq/kg to ^{210}Pb and will be used to measure the PTFE.

The collaboration will continue assaying all materials used in the detector as they are designed and procured. We anticipate completing assays for all these items with LZ-specified materials and assembling a detailed background model prior to the start of integration and assembly. The impact of these backgrounds is presented in Table 9.2.7.

9.2.2 Backgrounds Table

Table 9.2.7 presents the impact of the background sources assembled in Table 9.2.1 as determined through Monte Carlo simulations with LZSim and by adopting the radio-activities as assayed by LZ or as expected based on literature values. The activities for the material components easily satisfies the LZ requirements and are also well below the goals, with a total contribution to background of under 0.1 NR events and 0.3 µdru in 1,000 d with a fiducial volume of 5.6 tonne of Xe. This is for a WIMP search region defined by a 3-fold PMT coincidence lower bound and 20 phd upper bound, equivalent to approximately 1.5 keV$_{ee}$ to 6.5 keV$_{ee}$, before

Table 9.2.6: NAA measurements of ^{40}K, ^{238}U, ^{232}Th, and ^{138}La activities in PTFE samples.

Values in (mBq/kg)				
	^{238}U ($\times 10^{-3}$)	^{232}Th ($\times 10^{-3}$)	^{40}K ($\times 10^{-3}$)	^{138}La ($\times 10^{-6}$)
PTFE8764	<42	13 ± 3	66 ± 4	2.8 ± 0.2
DuPont 807NX	38 ± 9	29 ± 2	96 ± 5	9.4 ± 0.5
DuPont NXT85	<21	28 ± 2	122 ± 10	6.4 ± 0.3
Flontech FLON008	<27	51 ± 3	329 ± 17	25 ± 1
PTFE8764 sheet	18 ± 4	29 ± 1	76 ± 1	8.5 ± 0.2

discrimination or NR efficiency is applied, but employing the spontaneous fission rejection power of LZ, OD and Xe skin vetoes, and single scatter requirements. This energy region, selected for evaluation of trial components, is functionally equivalent to that employed in the full PLR when considering the experiment's optimum sensitivity.

Most of the entries in Table 9.2.7 are formed from composite materials, where more than 130 components or subcomponents contribute to make up the different elements. A comprehensive table that includes separate sections for each detector element detailing each subcomponent is maintained in a version-controlled archive; Table 9.2.7 is the summary from the complete table. The assayed contamination values are used to generate mass-weighted average activities for Monte Carlo simulations for ER backgrounds, and in major components all the individual materials are used to generate NR rates from (α,n) and spontaneous fission neutrons. Neutron emission rates in the simulations include contributions from ^{210}Pb at measured values for both the TPC PMT bases and skin PMT bases. For several components 90 % C.L. upper limits have been set for ER rates where simulations are statistics limited given the lack of any recoils in the xenon that pass selection criteria. Where background is generated by some isotopes, such as ^{238}U or ^{235}U, but not others, such as ^{40}K, mean values and upper limits are combined. This occurs in cases where either components are located far from the xenon target, are situated where radiation released is vetoed with very high efficiency, or where contamination levels are so low that no background is generated on timescales several times the LZ exposure. The components in Table 9.2.7 where this is the case, and reported ER counts include a significant rate from an upper limit, are the R8520 skin PMT bases and the HV Conduit and Cables.

There are several contributors to background in addition to the ER and NR counts induced by fixed radioactivity in materials. Radioactivity associated with radon emanated into the instrument is expected to contribute approximately 840 counts to the ER events, where half of this comes from materials and the rest from radon released from dust on material surfaces. This level of background, discussed in Section 9.5, is based on conservative estimates for emanation from materials and from dust. The activity, 2 µBq/kg, corresponds to a total of approximately 20.2 mBq from ^{222}Rn dispersed throughout the xenon target, which is at the level of our requirements (20 mBq). A total of 20 mBq in the xenon corresponds to 13.4 mBq from ^{222}Rn in the active volume and 11.2 mBq in the fiducial target. We do not expect a contribution from ^{220}Rn in LZ. However, due to the observation of a population of alphas attributed to ^{220}Rn in LUX, where radon mitigation was minimal, we nonetheless conservatively include a rate from a 0.1 µBq/kg concentration of ^{220}Rn in our background estimates.

We anticipate the decay-daughters from ^{222}Rn to accumulate on the surfaces of the detector during manufacturing and assembly. LZ has taken steps to minimize this plate-out deploying clean rooms and Rn-reduced air for some of the critical assembly tasks. Several large volume liquid scintillator experiments [18, 19] reported observing mobility of these products, in particular ^{210}Bi. The untagged beta decay would present an ER background similar to the ^{222}Rn. Studies were conducted to look for the mobility of ^{210}Bi in LUX data. Severe limits obtained from LUX, when applied to the LZ plate out requirement, place an upper limit on the ^{210}Bi of 0.1 µBq/kg, resulting in a limit of 40 ER counts. We have explicitly added an entry in the table for this background source.

As discussed in Section 9.2, we maintain a goal for total activity from radon emanation in the xenon of 1 mBq. This would lower the contribution from radon emanation to 1 µdru, matching goals for krypton and from fixed material radioactivity. Contributions from Kr and Ar, with 27 counts, are discussed in Section 9.7. Laboratory and cosmogenic backgrounds contribute just 4.3 ER and 0.06 NR background events, well below goals for fixed material radioactivity; these backgrounds are discussed in Section 9.8. Finally, surface contamination on materials is described in Section 9.6. This generates both ER and NR counts at the level of 0.19 and 0.37, respectively, from intrinsic radioactivity in the dust and backgrounds due to radon plate-out.

Contributions from the irreducible physics sources are discussed in Section 2. These include ER contributions from the double beta decay of ^{136}Xe and astrophysical neutrinos, in particular pp and ^{7}Be solar neu-

Table 9.2.7: Estimated background counts in the WIMP search region of interest, as discussed in the text, from all significant sources in the LZ 1,000 d exposure. Mass-weighted average activities obtained from Table 9.2.1 are shown for composite materials. Solar ^{8}B neutrinos are expected to contribute (7 ± 3) NR but only at very low energies and are excluded from the table.

	Mass	$^{238}U_e$	$^{238}U_l$	$^{232}Th_e$	$^{232}Th_l$	^{60}Co	^{40}K	n/yr	ER	NR
	(kg)	mBq/kg							(cts)	(cts)
Upper PMT Structure	40.5	3.90	0.23	0.49	0.38	0.00	1.46	2.53	0.05	0.000
Lower PMT Structure	69.9	2.40	0.13	0.30	0.24	0.00	0.91	6.06	0.05	0.001
R11410 3" PMTs	91.9	71.6	3.20	3.12	2.99	2.82	15.4	81.8	1.46	0.013
R11410 PMT Bases	2.8	288	75.8	28.4	27.9	1.43	69.4	34.7	0.36	0.004
R8778 2" Skin PMTs	6.1	138	59.4	16.9	16.9	16.3	413	52.8	0.13	0.008
R8520 Skin 1" PMTs	2.2	60.5	5.19	4.75	4.75	24.2	333	4.60	0.02	0.001
R8520 PMT Bases	0.2	213	108	42.2	37.6	2.23	124	3.62	0.00	0.000
PMT Cabling	104	29.8	1.47	3.31	3.15	0.65	33.1	2.65	1.43	0.000
TPC PTFE	184	0.02	0.02	0.03	0.03	0.00	0.12	22.5	0.06	0.008
Grid Wires	0.8	1.20	0.27	0.33	0.49	1.60	0.40	0.02	0.00	0.000
Grid Holders	62.2	1.20	0.27	0.33	0.49	1.60	0.40	6.33	0.27	0.002
Field Shaping Rings	91.6	5.41	0.09	0.28	0.23	0.00	0.54	10.8	0.23	0.004
TPC Sensors	0.90	21.1	13.5	22.9	14.2	0.50	26.3	24.8	0.01	0.002
TPC Thermometers	0.06	336	90.5	38.5	25.0	7.26	3360	1.49	0.05	0.000
Xe Tubing	15.1	0.79	0.18	0.23	0.33	1.05	0.30	0.64	0.00	0.000
HV Components	138	1.90	2.00	0.50	0.60	1.40	1.20	4.90	0.04	0.001
Conduits	200	1.25	0.40	2.59	0.66	1.24	1.47	5.33	0.06	0.001
Cryostat Vessel	2410	1.59	0.11	0.29	0.25	0.07	0.56	124	0.63	0.013
Cryostat Seals	33.7	73.9	26.2	3.22	4.24	10.0	69.1	38.8	0.45	0.002
Cryostat Insulation	23.8	18.9	18.9	3.45	3.45	1.97	51.7	69.8	0.43	0.007
Cryostat Teflon Liner	26	0.02	0.02	0.03	0.03	0.00	0.12	3.18	0.00	0.000
Outer Detector Tanks	3200	0.16	0.39	0.02	0.06	0.04	5.36	78.0	0.45	0.001
Liquid Scintillator	17600	0.01	0.01	0.01	0.01	0.00	0.00	14.3	0.03	0.000
Outer Detector PMTs	205	570	470	395	388	0.00	534	7590	0.01	0.000
OD PMT Supports	770	1.20	0.27	0.33	0.49	1.60	0.40	14.3	0.00	0.000
Subtotal (Detector Components)									6.20	0.070
^{222}Rn (2.0 µBq/kg)									722	-
^{220}Rn (0.1 µBq/kg)									122	-
^{nat}Kr (0.015 ppt (g/g))									24.5	-
^{nat}Ar (0.45 ppt (g/g))									2.47	-
^{210}Bi (0.1 µBq/kg)									40	-
Laboratory and Cosmogenics									4.3	0.06
Fixed Surface Contamination									0.19	0.37
Subtotal (Non-ν counts)									922	0.50
^{136}Xe $2\nu\beta\beta$									67	0.00
Astrophysical ν counts (pp + ^{7}Be + ^{13}N)									255	0.00
Astrophysical ν counts (^{8}B)									0.00	0.00
Astrophysical ν counts (hep)									0.00	0.21

(continued on next page)

	Mass (kg)	$^{238}U_e$	$^{238}U_l$	$^{232}Th_e$	$^{232}Th_l$	^{60}Co	^{40}K	n/yr	ER (cts)	NR (cts)
		mBq/kg								
Astrophysical ν counts (diffuse supernova)									0.00	0.05
Astrophysical ν counts (atmospheric)									0.00	0.46
Subtotal (Physics backgrounds)									322	0.72
Total									1,244	1.22
Total (with 99.5 % ER discrimination, 50 % NR efficiency)									6.22	0.61
Sum of ER and NR in LZ for 1,000 d, 5.6 tonne FV, with all analysis cuts									**6.83**	

trinos. Solar ^{8}B and hep neutrinos, together with atmospheric and diffuse supernovae neutrinos contribute to NR background through coherent neutrino-nucleus scattering. As described in Section 2, (7 ± 3) NR are expected from Solar ^{8}B neutrinos. However, these are at very low energies and are therefore excluded from Table 9.2.7.

The total expected background to the WIMP search in LZ under the assumption of 99.5 % discrimination against ERs and 50 % NR acceptance is 6.8 counts.

9.3 Techniques and Sensitivities

The LZ project will require approximately 500 materials assays, determined by counting materials, parts and components detailed in the project's CAD drawings. This is consistent with expectations based on our experience from LUX, EXO, and other similar low-background experiments when including multiple techniques and confirmation measurements. As already discussed we have achieved good success for major items through completed assays. ICP-MS, HPGe, NAA and Radon Emanation systems will all be utilized, as no single technique has sensitivity to all radioactive isotopes within all materials, nor can any single technique at present provide sensitivity to the full ^{238}U and ^{232}Th decay chains. Use of all four techniques will provide the required accurate model of a material's full γ-ray, neutron and beta emission, and the subsequent impact on the radiation budget and sensitivity of the experiment. Any rare-event search would benefit from the availability of all techniques, which vary in their sample throughput and screening duration, requirements for sample size, access to instruments, ability to do bulk screening of complete components, and preservation or destruction of samples in the assaying process. Table 9.3.1 provides a summary of these assay techniques.

Sensitivity to U and Th decay chain species down to $\approx$10 ppt has been demonstrated using ultralow-background HPGe detectors. HPGe can also assay ^{60}Co, ^{40}K, and other radioactive species emitting γ-rays. This technique is nondestructive and, in addition to sample screening, finished components can be assayed prior to installation. Under the assumption of secular equilibrium, with all isotopic decays remaining within the same volume, the activity and concentration for any particular isotope in the chain may be inferred from the measured U and Th content, assuming natural terrestrial abundance ratios. However, secular equilibrium can be broken through removal of radioactive isotopes during chemical processing or through emanation and outgassing. HPGe readily identifies the concentrations of isotopes from mid- to late-chain isotopes from the early chain decays of ^{238}U and ^{232}Th, particularly those with energies in excess of several hundred keV. Background-subtracted γ-ray counting is performed around specific energy ranges to identify radioactive isotopes. Taking into account the detector efficiency at that energy for the specific sample geometry allows calculation of isotopic concentrations. A typical assay lasts 1 to 2 weeks per sample to accrue statistics at the sensitivities required for the LZ assays. These direct γ-ray assays probe the bulk of the radioactivity from any material, including identification of equilibrium states. The instruments available to the project are described in Section 9.4.1, and will be used to assay all materials. The HPGe technique is less sensitive,

Table 9.3.1: Primary material radio-assay techniques, indicating isotopic sensitivity and detection limits, as well as typical throughput or single-sample measurement duration.

Technique	Isotopic Sensitivity	Typical Sensitivity Limits	Sample Mass	Sampling Duration	Destructive/Non-destructive and Notes
HPGe	^{238}U, ^{235}U, ^{232}Th chains, ^{40}K, ^{60}Co, ^{137}Cs any γ-ray emitter	50 ppt U, 100 ppt Th	kg	Up to 2 weeks	Non-destructive, very versatile, not as sensitive as other techniques, large samples
ICP-MS	^{238}U, ^{235}U, ^{232}Th (top of chain)	10^{-12} g/g	mg to g	Days	Destructive, requires sample digestion, preparation critical
NAA	^{238}U, ^{235}U, ^{232}Th (top of chain), K	10^{-12} g/g to 10^{-14} g/g	g	Days to weeks	Destructive, sensitive to some contaminants
GD-MS	^{238}U, ^{235}U, ^{232}Th (top of chain)	10^{-10} g/g	mg to g	Days	Destructive, minimal matrix effects, cannot analyze ceramics and other insulators
Radon Emanation	^{222}Rn, ^{220}Rn	0.1 mBq	kg	1 to 3 weeks	Non-destructive, large samples, limited by size of emanation chamber

however, to the progenitor isotopes or the low-energy or low-probability γ-ray emission from decays in the early chain [20].

ICP-MS offers very precise determination of elemental contamination with potentially up to 100× better sensitivity for the progenitor U and Th concentrations compared to γ-ray spectroscopy. Since ICP-MS directly assays the ^{238}U, ^{235}U, and ^{232}Th progenitor activity it informs the contribution to neutron flux from (α,n) in low-Z materials, but also the contribution from spontaneous fission, which in specific materials can dominate. However, it is limited in identifying daughter isotopes in the U and Th decay chains that are better probed by HPGe. The ICP-MS technique assays very small samples that are atomized and measured with a mass spectrometer. As a destructive technique, it is not used on finished components. The limitation of ICP-MS is that the sample must be soluble - typically in mixtures of HF, HCl, and HNO_3- and that several samples from materials must be screened to probe contamination distribution and homogeneity. Assays take 1 d to 2 d per material, dominated by the sample preparation time, where extreme care must be taken to avoid contamination of solvents and reactants. ICP-MS will be used to provide confirmation of the direct γ-ray counting assays, and inform the background model with potentially significant contributions from the tops of the U/Th chain inaccessible to γ-ray measurements; particularly important for constraining systematic uncertainties in the PLR for signal identification. It will also provide chemical compositions to improve cal-

culations of neutron emission yields from materials. Finally, ICP-MS available to the LZ project mitigates potential throughput limitations in long duration underground assays, with rapid direct U/Th measurements that can be used to establish background contributions under assumptions of secular equilibrium through the decay chains. This may be particularly useful for small/low-mass components that need rapid assessment, since they can be performed and material cleared for use before the γ-ray assays that will determine the bulk of the radio-content with sensitivity to equilibrium states are performed. The LZ ICP-MS systems are presented in Section 9.4.2.

Neutron activation analysis (NAA) achieves sensitivities up to 1,000× better than direct counting. Samples are irradiated with neutrons from the reactor to activate some of the stable isotopes, which subsequently emit γ-rays of well-known energy that are detected through γ-ray spectroscopy. Elemental concentrations are then inferred, using tabulated neutron-capture cross sections convoluted with the reactor neutron spectra. Samples must be specially prepared and compatible with neutron irradiation in a reactor, and then measured with surface γ-ray counters. NAA probes the bulk contamination simultaneously and is not limited by the composition of the material since no sample digestions or ablations are required. Indeed, of all known techniques, NAA can provide the best sensitivity to U and Th concentration. However, concurrent activation of trace contaminants of little interest or from the primary constituents of the sample can produce high γ-ray fluxes that present a background to the U and Th measurements, severely compromising sensitivity. Counting can be timed to allow interfering species to decay, allowing identification of the isotopes of interest with high accuracy. As with ICP-MS, this technique requires small sample masses, does not assay finished components, and assumptions of secular equilibrium need to be made since this technique measures the top of the U and Th chains. NAA is particularly useful for materials with very low activities difficult to assay directly with γ-ray counting, and also difficult to digest for ICP-MS. The PTFE in the LZ detector represents one such material. The proximity of the PTFE to the active Xe, both in defining the TPC and around the PMTs, coupled to a high (α,n) cross section, sets stringent constraints on the acceptable U and Th content. As described in the previous subsection, NAA has been successfully utilized to identify suitable material for the LZ project, with details of the facility presented in Section 9.4.3.

Particular attention must be paid to radon, as it is a noble gas consisting solely of radioactive isotopes, is produced in the decay chains of uranium and thorium, and has the ability to enter Xe volumes due to its chemical inertness and subsequent long diffusion lengths through solids. Outgassing of radon from a material in which it has been produced is commonly termed "radon emanation". Especially for materials in contact with or in close proximity to Xe, radon emanation must be taken into account in setting the levels of U/Th that can be tolerated (with stringent limits particularly on U) due to the presence of ^{222}Rn in the ^{238}U decay chain, as well as ^{220}Rn from ^{232}Th decay. LXe cannot provide self-shielding against the dispersed Rn, unlike radioactivity from fixed contaminants. Radon emanation from the bulk of a material may be estimated once its U/Th decay chain content (in particular its ^{226}Ra content) has been assayed using HPGe detectors. However, such estimates must be supplemented by direct screening for radon emanation for critical materials due to limited sensitivity in HPGe, systematic error from assumptions on equilibrium chain states, uncertainties in describing temperature-dependent radon transport in materials, and uncertainties on the amount of contaminants near surfaces. Direct measurements are performed by allowing bulk materials, either large samples or finished components, to emanate radon within a sealed chamber for a period of one or more weeks. The radon is then transferred using a carrier gas such as He or N_2 with high efficiency to a detector system, where radon progeny is detected through its radioactive decay, either using alpha counting or γ-rays. The four radon emanation systems available to LZ all meet requirements, with sensitivity ranging from 0.1 mBq to 0.3 mBq. These systems are presented in Section 9.5.

Most of the facilities for the direct assaying measurements are operated directly by LZ groups or exist at LZ institutes, allowing us to maintain control of sample preparation, measurements, analysis, and interpretation of data necessary to ensure sufficient sensitivity with reliable reproducibility and control of systematics.

Commercial facilities that provide Glow Discharge Mass Spectrometry (GD-MS) are available to the collaboration. GD-MS has poorer sensitivity (≈0.1 ppb U/Th) than ICP-MS, can only be used with conductive or semiconductive solids, and commercial service providers are typically limited in sensitivity due to regular exposure of their instruments and sample preparation infrastructure to materials with high concentrations of contaminants. However, it may be exploited for additional throughput or rapid confirmation of measurements if necessary.

9.4 Intrinsic Contamination Techniques and Devices

Identification of key materials presented in Section 9.2.1 with ultra-low activity assays for intrinsic contamination demonstrate existing instrument sensitivity and capabilities within the project. Here we present the instruments and facilities used to perform the fixed contaminant assays used already and available to the project to meet the both throughput and sensitivity requirements to schedule. The materials assay schedule includes all instruments described below, and is managed through the project to allow flexibility by assigning resources depending on sample type, size, required sensitivity, timescale, and risk. The project has performed cross-calibration campaigns of our instruments that have included circulating standard sources, blind samples, and exchanging data and analysis routines, to ensure reliability across our assays.

9.4.1 HPGe

Eleven HPGe detectors located in facilities both above- and underground are available to the LZ collaboration, with differences in detector types and shielding configuration providing useful dynamic range both in terms of sensitivity to particular isotopes and physical sample geometries. All of the instruments, with several previously used for LUX or ZEPLIN, are managed and operated by LZ collaborating institutes and are already in use for the LZ material screening campaign. The detectors are typically several hundreds of grams to several kilograms in mass, with a mixture of n-type, p-type, and broad energy Ge (BEGe) crystals, providing relative efficiencies at the tens of percent through to in excess of 100 % (as compared to the detection efficiency of a (3 × 3)-inch NaI crystal for 1.33 MeV γ-rays from a ^{60}Co source placed 25 cm from the detector face). While p-type crystals can be grown to larger sizes and hence require less counting time due to their high efficiency, the low energy performance of the n-type and broad energy crystals is superior due to less intervening material between source and active Ge. Clean samples are placed close to the Ge crystal and sealed for several days to weeks in order to accrue sufficient statistics, depending on the minimum detectable activity (MDA). The detectors are generally shielded with low-activity Pb and Cu, flushed with dry nitrogen to displace the Rn-carrying air, and sometimes are surrounded by veto detectors to suppress background from Compton scattering that dominates the MDA for low-energy γ-rays. To reduce backgrounds further, most of the detectors are operated in underground sites, at SURF within the Black Hills State University Underground Campus (BHUC), and at the U.K. Boulby Underground Laboratory within the Boulby Germanium Suite (BUGS), lowering the muon flux by several orders of magnitude. We also retain a number of surface counters that are particularly useful for pre-screenings before more sensitive underground assays. All of the HPGe detectors available to LZ are shown in Table 9.4.1.

9.4.1.1 BHUC

The BHUC is a dedicated facility for low-background counting at SURF and was completed in late 2015. Four ultra-low background HPGe detectors are operational: MAEVE, MORGAN, MORDRED, and SOLO. MAEVE, formerly situated at Oroville before operations in the Davis campus at SURF and final re-location in the BHUC, is an 85 % p-type HPGe detector in a low-activity Pb- and Cu-shielded and Rn-flushed chamber.

Table 9.4.1: γ-ray-counting facilities available for LZ material radio-assays. Sensitivities shown are approximate detectable activities after 2 weeks of counting and samples of order-kg mass. Typical cavity size within the shielding of these detectors within which samples may be placed is 0.03 m^3.

Detector	Site	Site Depth (mwe)	Crystal Type	Crystal Mass (Relative Eff)	Sensitivity, U (mBq/kg)	Sensitivity, Th (mBq/kg)
Chaloner	Boulby	2805	BEGe	0.8 kg (48 %)	0.6	0.2
Ge-II	Alabama	0	p-type	1.4 kg (60 %)	4.0	1.2
Ge-III	Alabama	0	p-type	2.2 kg (100 %)	4.0	1.2
Lumpsey	Boulby	2805	Well	1.5 kg (67 %)	0.4	0.3
Lunehead	Boulby	2805	p-type	2.0 kg (92 %)	0.7	0.2
Maeve	SURF	4300	p-type	1.7 kg (85 %)	0.1	0.1
Merlin	LBNL	180	n-type	2.3 kg (115 %)	6.0	8.0
Mordred	SURF	4300	n-type	1.2 kg (60 %)	0.7	0.7
Morgan	SURF	4300	p-type	2.1 kg (85 %)	0.2	0.2
SOLO	SURF	4300	p-type	0.6 kg (30 %)	0.5	0.2
Wilton	Boulby	2805	BEGe	0.4 kg (18 %)	7.0	4.0

The MAEVE shield was recently upgraded with the addition of a layer of very old Pb shielding. For several kg sized samples, the sensitivity after a week of counting reaches approximately 10 ppt U (≈0.1 mBq/kg ^{238}U) and 25 ppt Th (≈0.1 mBq/kg ^{232}Th), 20 ppb for K (≈0.7 mBq/kg ^{40}K) and ≈0.03 mBq/kg for ^{60}Co. Nearly an identical detector, MORGAN, was paired with MAEVE in 2015, and is now fully operational.

LBNL upgraded the CUBED detector, now called MORDRED with a low background cryostat and improved design. MORDRED has a 1.2 kg ORTEC n-type coaxial HPGe detector with a 254 cm^3 active volume and a relative efficiency of 60 %. The sample chamber, with a dimension of 8,000 cm^3, is surrounded by a 10 cm-thick 99.9 % OFHC copper shield, enclosed in a stainless steel box that is itself sealed by 10 cm of lead. MORDRED achieves similar performance to MAEVE and MORGAN, and as an n-type detector will aid in measuring early U chain and ^{210}Pb.

The SOLO detector, formerly operated at Soudan Mine, has also been moved to BHUC. The SOLO shielding houses a nitrogen-flushed Pb shield that has a minimum thickness of 30 cm 50 Bq/kg ^{210}Pb activity) with a 5 cm inner liner of 150 y-old low-activity Pb (50 mBq/kg ^{210}Pb activity). A counting chamber of 8,000 cm^3 contains the 0.6 kg "Diode M" HPGe detector. This detector approaches sensitivities at the 50 ppt level for ^{238}U and ^{232}Th and 25 ppb for ^{40}K for multi-kg samples.

The LBNL group manage and operate the BHUC counters for the LZ project. MAEVE delivers the best sensitivity of all the project's detectors, and MORDRED will extend the facilities low-energy sensitivity as an n-type detector. The SOLO and MORGAN detectors are reserved with 100 % live-time screening of LZ PMTs following delivery in 2016. The BHUC detectors, together with surface and Boulby counters, meet the LZ project's expected throughput demands with MDA's sufficient for most materials used in the construction of LZ. However, it is anticipated that additional counters will be added to the array in 2016 from the South Dakota School of Mines and Technology (SDSMT), UC Berkeley, and the University of South Dakota (USD).

9.4.1.2 BUGS

The Boulby Underground Facility, at 2,805 mwe, has been upgraded through 2015 to now include a dedicated low-background counting area that is operated as an ISO Class 6 cleanroom [21]. The Boulby Under-

ground Germanium Suite (BUGS) is housed in this area and includes three primary high sensitivity ultra-low background detectors: Chaloner, Lunehead, and Lumpsey, and a fourth pre-screener: Wilton. The primary detectors are each housed in custom-built lead and copper shields using existing Boulby stock material. The shields feature a retractable roof to aid the reproducibility of backgrounds. The shield cavities range between 30 l to 40 l, and are purged with N_2 gas fed directly into the inner cavity to reduce the ambient radon activity from 3 Bq/m^3 to negligible levels. The shields allow detectors to be retracted and interchanged, allowing detector maintenance without dismantling, and matching of instruments to castles to optimize sensitivity across the suite.

The Chaloner BEGe detector is a Canberra BE5030 (0.8 kg Ge, 48 % relative efficiency) installed in 2014. The crystal is configured in a unique planar geometry, yielding greater peak-to-Compton ratios at the γ-ray energies of interest, and improved energy resolution (by ≈30 % over typical p-type detectors at 122 keV). BEGe detectors also have considerably lower energy thresholds due to a factor-70 reduction in dead layer thickness on the front face of the Ge crystal and the utilization of a carbon-fiber end-cap window. These factors provide useful efficiency down to 10 keV (as opposed to ≈80 keV for p-type HPGe detectors) and consequently can directly measure ^{210}Pb a problematic source of background that is particularly difficult to quantify with other techniques. The BE5030 achieves <50 ppt sensitivity to ^{238}U and ^{232}Th for typical samples despite the low relative efficiency given the geometry and high resolution of the crystal. The energy range of the BEGe also gives us (unique to such a screening program) information about the elemental content of some materials through x-ray fluorescence. This has proved particularly useful in verifying composition of sample of candidate capacitors, found to contain $BaTiO_3$, as the detector is sensitive to fluorescence x-rays from barium, rather than Al_2 O_3 .

The Lunehead detector is a GEM-XX240-S p-type HPGe of 92 % relative efficiency. Used extensively for the ZEPLIN-III experiment [22], this detector has undergone complete refurbishment. With the exception of the Ge crystal, the detector has been overhauled and retrofitted with ultra-low-background components in 2014 to become a GEMXX-95-LB-C-HJ model with J-type neck and carbon fiber entrance window. Lunehead achieves sensitivity to about 50 ppt of ^{238}U and ^{232}Th.

The Lumpsey detector is a Canberra SAGe Well-type ultra-low-background GSW275L7950-30U-ULB instrument. Lumpsey has a 1.5 kg crystal that operates as a conventional co-axial (p-type) detector for large samples, with approximately 40 keV threshold, and sensitivity equivalent to the Chaloner and Lunehead detectors. However, the crystal includes a 28 mm diameter, 40 mm cavity ('well') where small samples can be placed. This provides unique capability with high sensitivity rapid screening of small components or materials by enveloping the sample with $> 3\pi$ coverage. The thin lithium contact inside the well allows low energy threshold at 20 keV, similar to the BEGe detectors. This is particularly important for measurement of the 46.5 keV γ-ray from the decay of ^{210}Pb. As described earlier, detection and mitigation of ^{210}Pb in bulk PTFE is required to mitigate (α,n) production on fluorine by ^{210}Po, a ^{210}Pb daughter nucleus. Traditional HPGe γ-ray counting, NAA, and ICP-MS cannot readily be applied to detect ^{210}Pb or its daughters at the mBq/kg level. Lumpsey demonstrates sensitivity of 35 mBq/kg for a small (30 g) sample after 21 d of counting and 10 mBq/kg for more massive samples after 50 d, meeting the project requirement for ^{210}Pb in bulk material screening. The Lumpsey well-detector will be used for the assays of PTFE for ^{210}Pb content.

The Wilton detector is a Canberra BE2825 with low mass (0.4 kg) BEGe crystal. Though Wilton is an ultralow-background instrument it has a straight neck from dewar to crystal, and is housed in a smaller flip-lid lead shield with tin and copper liner. Wilton is used as a pre-screener, where samples are first assessed in a 1 to 2 day measurement. Wilton's sensitivity is at the level of 7 mBq/kg to ^{238}U and 4 mBq/kg to ^{232}Th. This allows materials with high radioactivity to be immediately rejected if requirements are not met, without disturbing the primary high-sensitivity instruments. Where samples are to be passed to the primary detectors, the pre-screener can inform screening times required to meet sensitivity for the assay.

BUGS is managed by the LZ groups at Oxford and UCL, through the DMUK consortium, with dedicated effort from Boulby providing significant operational and infrastructure support. The instruments have already been used extensively through the project's R&D phase and beyond to perform critical assays in particular to identify PMT base materials, cryostat materials, and support PMT construction material assays with SOLO and MAEVE. The Chaloner and Lunehead detectors are reserved exclusively for screening of PMTs, begun in mid-2016.

9.4.1.3 Surface HPGe Detectors

The MERLIN detector, as with Wilton at Boulby, is used to pre-screen materials and determine suitability for underground assaying and required sampling livetime. Materials identified as exceeding requirements by MERLIN are not assayed with the high sensitivity counters in the BHUC. MERLIN is a 115 % relative efficiency n-type low-background HPGe operated at the surface Berkeley Low Background Facility (BLBF) within a 4π shielded room with 1.5 m-thick low-activity serpentine rock concrete walls. The HPGe detector head is mounted on a J-hook to reduce line-of-sight for background from electronics and the cryostat, and is shielded in a Pb and OFHC Cu castle. It has an MDA of approximately 0.5 ppb (6 mBq/kg) to ^{238}U for O(kg) samples from 1 d of counting, and 2 ppb (8 mBq/kg) for ^{232}Th. Sensitivity to K and ^{60}Co is at the level of 1 ppm and 0.04 pCi/kg, respectively.

Finally, the University of Alabama operates two high sensitivity low-background HPGe detectors at its surface screening facility: the Ge-II and Ge-III detectors. Each detector is housed in a lead-copper-shield equipped with an active cosmic-ray veto systems. The shield cavities are suitable for large samples. These devices can reach 0.3 ppb MDA for ^{238}U and ^{232}Th with two weeks of counting, useful for many LZ components, and also provide pre-screening. These detectors are essential for the NAA screening program for LZ, described in Section 9.4.3.

9.4.2 ICP-MS

The UCL group operate an ICP-MS facility dedicated to the LZ project [21]. At UCL, An ISO Class 6 cleanroom, erected in late 2015, contains all instruments and the sample preparation areas. The primary instrument is an Agilent 7900 ICP-MS, with sensitivity to U and Th below 10^{-12} g/g, allowing assay of materials with U and Th content at the level of a several ppt. The ICP-MS has an integrated auto-sampler for high speed discrete sample uptake with low-flow, Peltier-cooled sample introduction system. The system octopole can provide species discrimination through interference removal either with kinetic energy discrimination (KED) in helium collision mode, or in reaction mode using H_2, in addition to running with no gas at all, which in some cases is sufficient for U and Th measurements. High-purity Ar, He, and H_2 gases (5N grade) are introduced to the system as carrier gas, collision cell gas, or reaction gas, respectively. The system has been fitted with an inert sample introduction kit such that a micro flow nebuliser and platinum skimmer and sampling cones are used to allow up to 20 % concentration of acid in samples introduced to the ICP-MS, including HF. Calibration of the system is performed using tuning solutions containing Li, Y, Tl, Co, and Ce, in 2 % HNO_3. The mass numbers 7 (Li), 89 (Y) and 205 (Tl) are tracked for stability, sensitivity, resolution and linearity for the integrated system across the mass range. The backgrounds at these masses allow sub-ppt sensitivity, <3 % relative standard deviation (RSD) in count rate over a 20 min stability measurement period, and detector resolutions of <1 %.

The limiting factors in realizing reproducible high throughput ppt sensitivity is clean sample preparation, requiring digestion apparatus and procedures, as well as cleanliness of acids, that do not contaminate samples. Sample preparation infrastructure has been procured to address these issues and mitigate risks. A Milestone EthosUP microwave digestion system is able to digest solid samples at high temperatures in closed containers in minutes; this cannot readily be achieved using open hot-plate technology since volatiles are lost, the open

vials may be contaminated depending on the ambient environment and handling, and low temperatures limit the digestion efficiency, further increasing exposure to background. The digestion oven also allows for the use of high quantities of HF that greatly simplifies digestion and, crucially, allows measurement of virtually all materials that are being considered for use in LZ. The quality of the reagents used in the sample material and, more importantly, analytical blank digestions further limit sensitivity through variations in contamination levels, even for ultra-pure commercial products. Milestone acid distillation and reflux systems have been installed for control of acid purity and reproducibility, and the laboratory includes a Veloia 18 MΩ water purifier. Finally, a Pyro-260 microwave ashing system allows the possibility of digestion of materials such as PTFE and acrylics that are not otherwise digested easily, and are required with low radioactivity levels inaccessible to HPGe, necessitating the need for NAA.

Protocols and methodologies for operations, sample handling, and digestions are largely based on established protocols and methodologies developed that demonstrate sub-ppt measurements [1, 23, 24] The cleanroom contains an ISO Class 4 laminar flow unit, and a fume cupboard with H+ filtration for sample handling. Digestion protocols with specific acid chemistries and heating profiles with microwave digestion on a material-by-material basis are also available for the EthosUP system following our R&D phase and microwave digestion routines developed in partnership with Milestone and U.K. operators Analytix Limited. Microwave energy couples directly to ions, rotating around the dipole to cause friction and release heat, such that acids with higher dipole moments absorb microwaves readily for fast and even heating of reactant solutions. The vessels used in these high pressure reactors, in contrast, are constructed from materials with low or no dipole moment, such as tetra-fluoromethoxy (TFM), making them transparent to microwaves. High pressures in these closed vessels allow acids to be heated beyond their boiling points, further aiding material sample digestion. Protocols for digestion of all materials within the R11410 PMT, for example, have been developed and successfully tested already. A mixture of HNO_3, HCl and HF at 220 degrees Celsius (reaching 30 bar) over 45 minutes is sufficient for complete dissolution of all component materials. The nitric acid is commonly used to digest organic material, HCl for Fe-based alloys due to ability to hold chloro-complex in solution, and HF used for decomposing silicates.

The UCL ICP-MS facility became fully operational in December 2015, and material assays began in early 2016 following the establishment of QC and QA procedures for consistency checks, calibrations, optimizing of cleaning procedures, and assessment of systematics. Sample assays for the LZ project have begun with initial assays of plastics and foams for the cryostat sub-system, achieving results consistent with HPGe assays with the BUGS detectors.

The Center for Underground Physics (CUP), S. Korea, operates an ICP-MS laboratory supporting a number low-background experiments, including LZ. The facility and operations are largely the same as those described for UCL above, including ISO 6 cleanroom, Agilent 7900, and identical microwave digestion system now on order. The instrument was made operational and staffed its 20 m^2 unidirectional-flow cleanroom (about 180 air changes per hour) in October of 2015. The ICP-MS is equipped for He collision mode with potential to add a Hydrogen line at a later date if a strong need arises. It is has a UHMI (gas-diltuion) introduction system which can help to optimize sample introduction load into the plasma and reduce water and reagent backgrounds. It also was purchased with cold-plasma capability allowing removal of particular interferences with high ionization potentials. This is particularly useful for measurement of ^{39}K which is severely limited by interference from $^{38}ArH^+$. The lab contains an in-house acid distillation system and water is supplied from a 500L/hr 18 MΩ building-wide supply as input to a Millipore Advantage A10 water-purifier.

Protocols for cleaning are generally very similar to those stated above, derived largely from the same sources of experience, but sample preparation has so far been restricted only to un-assisted open digestion. Particular attention has been paid to quantifying and understanding the ultimate limits of measurement backgrounds, based largely on previous work performed at the University of Seoul. Using Savillex

brand digestion vessels, cleaning procedures consistent with descriptions above,and statistical subtraction of sample-dependent continuous backgrounds described by Ref. [25], CUP achieves blank contaminants of U and Th statistically consistent with zero (in the blanks this level can be at or below a few fg/g but increases for high concentration samples), and with sample limits significantly below the background equivalent level. A figure of merit using the calibration response, the measured background rate, and simple propagation of statistical errors is used to accurately predict sensitivities in a particular sample based on results of initial in-matrix tuning. Three sigma detection capability below 2 ppt has been demonstrated, but not yet pursued for a sufficiently pure material. Details depend on the sample chemistry, but similar levels are reasonable to expect for most easily acid-dissolvable samples such as metals.

These measurements take significant time owing to the need for high statistics, standard addition calibration of high-concentration samples, and frequent machine cleaning. For more routine measurements, the backgrounds are simply monitored and reported as an equivalent concentration, and lower concentration samples allow for external calibrations and a significantly relaxed cleaning schedule, allowing to measure less demanding samples at the rate of several per day with sensitivities to U and Th on the order of a few hundred ppt. Finally some initial work has been done to develop measurements of potassium using the cold plasma configuration, leading to measurements of a few hundred ppb of K, and to indications of potential sensitivity much lower, but not yet explored.

ICP-MS facilities are also available Black Hills University Campus, and at the University of Alabama. BHUC also operate an Agilent 7900, with additional laser ablation sample introduction capability with an ESI NWR 213 system. The system is housed in an ISO 7 clean area within a dedicated ICP-MS laboratory. The University of Alabama group have access to a Perkin-Elmer SCIEX-ELAN 6000 ICP-MS within the Geology department that has demonstrated capability to detect U/Th down to the level of tens of ppt and has availability to screen tens of samples on the timescale of a few months. This facility does not, however, provide services for sample digestion and separation/concentration of U/Th content. The Alabama group has carried out a systematic program to certify the capability of the facility, develop protocols to prepare samples for analysis without risk of cross-contamination, and set up a laboratory where common digestion and separation/concentration procedures can be performed.

9.4.3 NAA

The University of Alabama group within the LZ collaboration utilizes the 5.5 MW_{th} MIT Reactor II (MITR-II) to perform neutron activation of samples and subsequent measurements with the Ge-II and Ge-III surface HPGe detectors described in Section 9.4.1.3. MITR-II is a double-tank reactor with an inner tank for light-water coolant moderator and an outer one serving as heavy-water reflector [26]. Two pneumatic sample insertion facilities are available. Steady-state thermal neutron fluxes of up to 5.5×10^{13} neutrons/s/cm^2 can be achieved. The sample insertion facilities can accommodate multiple samples that range in size but are typically a few mm in diameter and several cm in length. The two sample insertion facilities offer differing thermal over fast neutron flux ratios. Sample irradiations ranging from minutes to days can be performed, allowing accumulation of very large neutron fluences, which is key for reaching high analysis sensitivity.

LZ samples are prepared, cleaned, and hermetically sealed at the University of Alabama in a cleanroom prior to activation. Polyethylene irradiation vials and samples are separately soaked in ultrapure HNO_3, rinsed and dried in a vacuum oven. Vials are welded shut with the clean samples within, and leak tested in a heated water bath. Irradiation at MITR-II is typically for about 10 h, with a NIST certified fly ash sample used to calibrate the neutron flux also irradiated for about 5 min. After activation, the samples can be recovered cleanly and safely to avoid any carry-over contamination problems from the activation vials or other instruments. The counting of the activated samples at Alabama utilizes a double differential time-energy analysis over a period of about 2 weeks. The typical shipping delay of 24 h is acceptable compared with the half-lives of the activation products of interest (such as ^{42}K, ^{233}Pa, and ^{239}Np). An exponential

decay is fit to each time series of activity, for each radionuclide over multiple time intervals. The activity is reported relative to an earlier reference time, by fitting the decay of each radionuclide with a known half-life for determining the composition of the sample. Elemental concentrations are inferred using tabulated energy dependent radiative neutron capture cross sections folded with a standard reactor neutron spectrum, where the model of the neutron flux assumes a thermal Maxwell-Boltzmann neutron energy distribution plus an epi-thermal tail.

The Alabama group routinely achieved 10^{-12} g/g sensitivity for Th and U using these techniques, as reported in [1], appropriate for the LZ material screening campaign. Indeed, NAA results obtained by the same group for the KamLAND experiment reached sensitivity to U and Th at the 10^{-14} g/g to 10^{-15} g/g level [1] for liquid scintillator. Requirements for assaying PTFE for the LZ project have already been met using NAA, as described in Section 9.2.1.

9.5 Radon Emanation

The background from radon emanation is dominated by the "naked" beta emission from ^{214}Pb in the ^{222}Rn sub-chain as it decays to ^{214}Bi, whereas the ^{214}Bi beta decay itself is readily identified by the subsequent ^{214}Po alpha decay that would be observed within an LZ event timeline ($T_{1/2}$ =160 µs). Similar coincidence rejection also occurs where beta decay is accompanied by a high-energy γ-ray, which may still be tagged by the LXe skin or external Gd-LS vetoes even if it leaves the active Xe volume. Radon-220 generates ^{212}Pb, which decays with a short-timescale Bi-Po (beta-alpha delayed coincidence) scheme similar to ^{214}Pb. Radon daughters are readily identified through their alpha decay signatures, as demonstrated in LUX, and can be used to characterize the ^{222}Rn and ^{220}Rn decay chain rates and distributions in the active region, providing a useful complement to estimating radon concentration from the beta decay contribution to the ER background. Indeed, these isotopes were the only sources of alpha decay identified in LUX [10]. As detailed in Table 9.5.2, there are multiple potential sources of radon emanation (e.g., PTFE reflectors, PTFE skin, PMT glass, PMT and HV cables, grid resistors, components in the circulation system), and radon emanation screening must be sensitive to sources that individually sustain smaller populations. We use 0.67 mBq in the active target within the TPC as the goal for ^{222}Rn, which equates to a steady-state population of approximately 300 atoms. This activity corresponds to 0.56 mBq in the fiducial LXe, and 1 mBq in the total amount of LXe. This activity results in a background contribution that matches those from Kr and from intrinsic material radioactivity, and is about 10 % of the irreducible pp solar neutrino background. Requirements for LZ are twenty times higher than these goals, with 20 mBq ^{222}Rn total, of which 13.4 mBq is in the active LXe, and 11.2 mBq in the fiducial LXe. This requirement ensures that the background due to radon does not dominate significantly over the irreducible pp solar neutrino background, so that the WIMP-search reach of the experiment is not significantly reduced. Background from ^{220}Rn is not expected given its very short half-life. Due to observation of an alpha population ascribed to ^{220}Rn in LUX, we conservatively include a contribution in our estimates. ^{220}Rn is required to contribute no more than than 20 % of the ER counts from ^{222}Rn.

All components that may contribute to the radon load within the LXe will be screened for radon emanation. These components include all that are within the inner cryostat or that come into direct contact with Xe during experimental operation. Some materials are screened to inform material selection. These assays are scheduled carefully in conjunction with material procurements. In other cases (such as the PMTs), the materials cannot be changed due to finite resources and schedule, but the assay is performed in order to inform the background model.

The LZ collaboration has extensive access to four radon-emanation screening stations that meet the sensitivity requirement for our assays. These are summarized in Table 9.5.1. In one of the stations, at Alabama, the radon atoms are collected by passing the radon-bearing gas through liquid scintillator, with the Bi-Po

Table 9.5.1: Radon-emanation facilities available for LZ material radio-assays. Sensitivities shown are approximate detectable activities after 2 weeks of emanation and counting. With the exception of the UCL system, all are managed by LZ groups. The UMd and Alabama systems are dedicated to LZ, while the UCL system is primarily for SuperNEMO, and the SDSM&T system will be shared (at <25 % time) with SuperCDMS.

Detector	Type	Detector Efficiency	Detector Background (mBq)	Samples/ Year	Chamber Volume (l)	Transfer Efficiency	Blank Rate (mBq)
UCL	PIN-diode	30 %	0.2	6	2.6 2.6	97 % 97 %	0.2 0.4
Maryland	PIN-diode	24 %	0.2	12	4.7	96 %	0.2
SDSM&T	PIN-diode	20 %	0.15	12 12	13 300	94 % 80 %	<0.3 0.3
Alabama	Liquid Scint.	40 %	<0.15	12 12	2.6 2.6	30 %	<0.4

coincidence detected through gated coincidence logic using one PMT viewing the scintillator. In the other three stations, radon atoms and daughters are collected electrostatically onto silicon PIN diode detectors to detect ^{218}Po and ^{214}Po alpha decays. One of these stations was developed at Case Western Reserve University and has been commissioned at the University of Maryland. Work at this system is focusing on emanation of systems that act as their own emanation chambers, such as plumbing for the LZ Xe recirculation system. The third station, at SDSM&T, has two emanation chambers including one large, 300-liter chamber that will be used to emanate large amounts of materials to achieve the best sensitivity. Finally, there is additional capability and throughput available in the U.K. using the system employed by the SuperNEMO group at UCL [27]. This system was used extensively in the R&D phase and LZ is expected to have access sufficient to measure emanation from six samples per year with it.

All stations were initially evaluated using calibrated sources of radon, with a cross-calibration program performed to ensure the accuracy of each system's overall efficiency and ability to estimate and subtract backgrounds. The first cross-calibration sample had a relatively high emanation rate, so that system efficiencies could be determined without possible interference from backgrounds. The second cross-calibration sample has a rate close to the quoted system sensitivities, to check the accuracy of background subtraction with the systems.

Screening a single sample for LZ takes about two weeks, including emanation and collection/detection times. Taking into consideration the desire for repeated measurements to check reproducibility and improve sensitivity, as well as runs to ensure stability of background rates and transfer efficiencies, no more than one sample per month per emanation chamber is planned for the scheduling of radon emanation screening.

In advance of the radon emanation screening, estimates were made of expected radon emanation from all materials in contact with the Xe, based on previous measurements of radon emanation from similar materials, or based on the combination of HPGe measurements of the bulk ^{226}Ra contamination together with measurements or estimates of Rn diffusion in the material. It must be noted that surface contamination may cause a higher rate of radon emanation from a material than is estimated from its bulk contamination, especially if the material's bulk is relatively radiopure or if the material has a very low radon diffusion constant. Table 9.5.2 summarizes the resulting radon budget from the critical materials. In cases where the dominant

Table 9.5.2: List of materials in contact with Xe, indicating the quantity of the material and the requirement for radon emanation from the material. This requirement is set by dividing the maximum activity from the materials, 10 mBq in the full 10 tons of LXe, evenly among the 9 major systems. A further 10 mBq from dust makes up the full requirement of 20 mBq from radon. The estimates of radon emanation are based either on direct assays (listed in boldface) or on the most similar object or material for which emanation rates are available in the literature. Some materials (labeled with *) are expected to emanate less radon when cold, but the estimate listed conservatively does not take such reduction into account. Only the estimate for PMT cables, as described in the text, takes this into account. We also list the quantity of material planned for screening. Expected reduction of radon by the carbon trap described in Section 6.4.5 is included in estimates for those components affected (labeled with †).

Material	Component(s)	Quantity	Unit	Requirement (mBq)	Estimate (mBq)	Screening Quantity
Al_2O_3 resistor	PMT Bases	9790	#	0.66	**0.58***	3,650
$BaTiO_3$ capacitor	PMT Bases	3010	#	0.66	**0.016***	100,000
Cirlex	PMT Bases	6000	cm^2	0.11	**0.37***	668
Titanium	Cryostat, PMT Mounts, Field Rings, Grid Supports	412,000	cm^2	1.70	0.41	550
PTFE	Reflectors, HV Umbilical	840,000	cm^2	0.66	**<1.3***	205,000
PMT Cabling†	PMT Cabling	17,000	m	0.55	0.09	3,000
PMT Feedthrough†	PMT HV Flange	122	#	0.11	**0.49**	5
PMT Feedthrough†	Signal Flange	88	#	0.11	**<0.24**	5
Steel Conduit†	Cabling Conduit	100,000	cm^2	0.22	0.055	100,000
R11410 PMT	R11410 PMT	488	#	1.10	1.26	488
R8520 PMT	R8520 PMT	90	#	0.47	0.15	90
R8778 PMT	R8778 PMT	36	#	0.08	0.09	36
Polyethylene	HV Umbilical	4200	cm^2	0.11	0.10	42,000
Tin-coated copper	HV Umbilical	11,000	cm^2	0.11	0.002	110,000
Tivar	HV Umbilical	3894	cm^2	0.22	0.004*	20,000
Acetal	HV Umbilical	195	cm^2	0.11	0.0002*	2000
Copper	HV Umbilical	39	cm^2	0.11	0.000007	400
Epoxy	HV Umbilical	1000	cm^2	0.11	0.0001*	10,000
Steel	Cryostat Seals, Xe Recirculation	135,000	cm^2	0.77	0.104	135,000
Recirculation Pump	Xe Recirculation	1	#	0.22	0.1	1
Purification Getter	Xe Recirculation	2.5	kg	1.10	1.34	2.5
Transducers & Valves	Xe Recirculation	30	#	0.44	0.17	30
Welds	Recirculation System, Cryostat	32.3	m	0.22	**0.11**	18.3
Dust				10.0	10.0	
Total				20.0	<16.9	

radon emanation is expected due to diffusion of radon from the material bulk, the expected radon emanation is based on room-temperature assays, conservatively ignoring the expected reduction of radon diffusion at LXe temperatures for all materials except the cables. For materials with low radon diffusion, such as metals, whose radon emanation is expected to be dominated by recoil punch-out, no emanation suppression is expected at reduced temperatures.

Without remediation, the cables would have been expected to be a major source of radon, emanating up to 30 mBq based on previous measurements [28]. This total would likely be dominated by the large surface area of the stainless steel braiding and contamination, such as dust, that is caught in this braiding. Mitigation of this large radon source will be achieved by adding a thin FEP cladding to the outside of the cables and by the installation of a carbon trap (described in Section 6.4.5) to filter radon out of the Xe gas from the conduits before it enters the main re-circulation. The cladding should make it easier to minimize contamination of the cables with dust. Furthermore, radon diffuses very slowly through the cold FEP cladding, nearly eliminating the emanation into the liquid Xe by the cables, while the trap will reduce the radon emanation into the gas portion of the conduits by at least 90 %. The combination of these two strategies reduces the expected emanation by the cables to 0.09 mBq. The carbon trap should significantly reduce the radon load from other room-temperature materials such as the PMT cable feedthroughs and conduits. Table 9.5.2 includes the expected reduction from the carbon trap.

Other potentially significant contributors were identified. Early assays of the components of the PMT bases indicate sufficiently low emanation even at room temperature that mitigation strategies, such as potting, need not be explored. The Xe purification getter material has been identified as a source of radon [29]. In order to minimize the radon emanation from the getter while allowing the high throughput needed by LZ, the baseline plan is to purchase a full-size getter cabinet with a partially-loaded getter cartridge (see Section 6.4.1). In addition, a screening program to identify a clean Zr substitute is underway, along with an investigation of other material options.

The largest single contributor to radon backgrounds in the experiment is expected to be due to dust on material surfaces. As described in Section 9.6.1, certified protocols for assembly and cleaning will provide the means to achieve a low enough dust concentration on materials in LZ. The dust is conservatively estimated to generate 10 mBq of activity. We assume that 25 % of ^{222}Rn from the dust on material surfaces escapes into the xenon; however preliminary measurements of of radon emanation from dust support fractions considerably lower (see Section 9.6.1).

The radon-emanation screening campaign, coordinated through dedicated management in the screening working group, extends beyond initial material selection. The system from SDSM&T will be relocated underground to SURF in order to screen large-scale assembled detector elements and plumbing lines. As pieces or sections are completed during installation of gas pipework for the LZ experiment, they will be isolated and assessed for Rn emanation and outgassing for early identification of problematic seals or components that require replacement, cleaning, or correction.

9.6 Surface Cleanliness

Once materials and components have met screening requirements and components have been procured, they will be kept clean during fabrication, storage, transport, and final assembly and integration into the experiment. We refer to this task as cleanliness. The major sources of contamination that must be addressed by the LZ cleanliness program are radon diffusion and daughter-nuclei plate-out, and dust and debris. Radon-daughter plate-out onto material surfaces may generate NR backgrounds through two mechanisms: (α,n) processes that release neutrons into the xenon; and ions from the ^{210}Pb sub-chain originating at the edge of the TPC being mis-reconstructed as NRs within the fiducial volume. ^{210}Pb on surfaces may also present ER background if it or daughters become mobile and enter the fiducial volume, with ^{210}Bi of note as a

beta-emitter. Dust on component surfaces carried into the xenon may produce ER and NR from intrinsic activity, as well as contributing significantly to the radon emanation background. We require that the effects of radon plate-out and dust deposition do not contribute to the background in LZ any more than the material components. Other sources of contamination must also be addressed, for example residual chemicals from fabrication processes, removal of which should be effected at the same time as cleaning to remove dust.

LZ draws on extensive cleanliness experience from earlier involvement in LUX, EXO, SNO, KamLAND, MAJORANA Demonstrator, and other low-background experiments to develop cleanliness protocols and assay techniques for dust and surface contamination. LZ is developing experiment-specific techniques for validating protocols and establishing a rigorous and comprehensive Quality Control (QC) and Quality Assurance (QA) program. All protocols and documentation are stored in the LZ information repository where they are linked to the specific material or component. No material or component will be integrated into the experiment without adequate documentation demonstrating handling following these protocols and successfully passing quality control tests.

In the following subsections we present details on the origins of these background sources; requirements and goals for both radon plate-out and dust depositions and equivalent maximum exposure times; controls and mitigation protocols; and assay techniques to ensure QC and QA certification.

9.6.1 Dust

Dust is typically characterized as fine-grained (<100 µm) material that results from the breaking/grinding of materials in the local environment. The specific content will reflect the location, but in general will include minerals from rock and soil, small amounts of plant pollen, human and animal hairs, textile fibers, paper fibers, human skin cells and even burnt meteorite particles. The contents and their relative proportions will determine the type and level of radioactivity, but in general the major contributors are ^{40}K, ^{238}U and ^{232}Th, all with activity levels around ∼10 mBq/g. Fine grains may easily become airborne, to be transported over significant distances, and then deposit on local surfaces. Electrostatic attraction allows vertical as well as horizontal surfaces to become contaminated. We expect to encounter dust in all locations where work is conducted, including the sourcing of materials where dust may become internalized to components, fabrication and construction phases, and in assembly and deployment. A detailed understanding of the radiological content of the dusts to be encountered has been developed, primarily through HPGe screening of floor sweepings and HEPA filter samples from the SURF underground areas. Measurements of the dust-particle count density, size, and deposition rate at SURF have also been completed [30] and will be extended to other assembly locations at LZ institutes and external sites where appropriate, such as the Ti-cryostat manufacturer.

The quantity of airborne dust in a specific location is found to vary significantly, with strong dependence on the local environment, geometry of any buildings, rate of airflow, and the use of air filtration to reduce the presence of dust, for example through the use of cleanrooms. The effectiveness of a cleanroom is highly dependent on associated procedures, for example the level of use, gowning procedures of users, and supplementary cleaning activities. The rate at which dust settles out on surfaces depends on the dust level in the air, the particle size distribution and density, and the rate of airflow. Where possible dust levels and dust deposition rates have been measured directly, but also modeling of these factors has been performed under a number of reasonable assumptions and model bases. We have developed two web–based calculators, denoted "SNO" and "ASML-Delft", respectively, that give allowed exposure times based on model and environmental inputs. The "SNO" model is based on the mass fallout model developed by R. Stokstad for SNO [31]. Input parameters include fresh air dust content, volume exchange rate, recirculation fraction, filter efficiency, and mass carry-in rate. "ASML-Delft" [32] is an empirical model derived from test measurements and validated by monitoring particle fallout rates as a function of air particle concentrations in operational cleanrooms in the semiconductor industry. Test measurements and operational cleanroom observations are consistent with parameterization to within an order of magnitude. As an example, the SNO model predicts

that a volume of fresh air (ISO class 8) that has 120 volume exchanges per hour including 0.8 % fresh air, and a carry-in rate of dust of 0.25 grams/d, would accumulate 500 ng/cm^2 of dust in a period of 2.3 days. The dust fallout rate is sensitive to the carry-in rate: for example, reducing the carry-in rate to 0.025 grams/d increases the accumulation time to 22 d. The carry-in rate is a factor that we control by implementation of cleanroom protocols. We are conducting a program of dust fall-out measurements within the LZ cleanrooms to determine actually realized rates under particular LZ conditions and locations. Our results indicate that fall-out rates are below those expected from the ASML-Delft models.

There are a number of mechanisms by which the radiological content of dust that is present on the surface of a component may be problematic. The relative importance of these varies depending on the properties and location of the component in the experiment. Contributions to ER and NR rates have been estimated based on the estimated levels of dust, known nuclear properties, and simulations propagating the decay products to the LZ experiment.

The most significant radiological concern for LZ from dust, and the one that drives our requirements, is radon emanation from dust within the inner cryostat and conduits. As previously described in Section 9.5, this contributes ERs via the naked beta decay of ^{214}Pb. The requirement for the total activity from radon emanation in the xenon is 20 mBq, with a goal of 1 mBq. Dust contributes half the rate in the requirement. Our present estimate is that the radon emanation from dust is equivalent to 10 mBq/g. This estimate is based on measured rates of radon emanation from naturally–occurring materials [33] and SNO reports on radon emanation from mine dust [34]. This sets the requirement on maximum amount of dust within the xenon at 1 g. We anticipate the contribution from dust will be significantly less given conservative estimates that define our requirements. Direct HPGe measurements we have performed to infer radon emanation from debris collected at SURF has indicated a 12 % radon emanation fraction, suppressed to 4 % at cryogenic temperatures due to reduced radon mobility. This is considerably lower than the 25 % we assume in defining our requirements. Direct radon emanation measurements of dust at room temperature will be performed end-2016. The goal for dust is a total of 10 mg within the xenon, corresponding to an activity of 0.1 mBq (based on the assumed 25 % emanation fraction). The total surface area from all components within and including the ICV is about 1.6×10^6 cm^2 and we conservatively set the required limit on dust surface mass density at 0.5 µg/cm^2. Our goal defines a density limit of 5 ng/cm^2. Dust on all other components is constrained to be at the same level, driven by the need to avoid cross contamination during assembly, however radon emitted from dust on non-wetted surfaces not in contact with any xenon is not a concern.

Beyond radon emanation, the intrinsic activity of dust generates both ER and NR background, and this contribution has also been evaluated in detail. Dust concentrations that meet requirements are assumed for the surfaces of all components within the ICV, taking into account the appropriate surface areas from the LZ CAD model. LZSim is used to generate radioactivity from these surfaces by propagating γ-rays and neutrons and estimating impact in LZ. These calculations account for (α,n) reactions on the appropriate targets. The range of few-MeV alpha particles in dust is on the order of 100 µm and thus in most decays it is reasonable to expect the alpha particle to escape. For a surface deposit, a simple geometric consideration predicts half of these to then impact the surface. Of particular concern is dust upon the surface of PTFE components, since the number of neutrons emitted for each incident alpha particle is particularly high for fluorine, 9.48 neutrons per 10^6 α-particles [35]. Aluminum also has a moderately high (α,n) cross section resulting in 0.63 neutrons per 10^6 α-particles. The (α,n) cross sections of other elements used in LZ all have significantly smaller cross sections. Of note, the design for the internal PTFE reflectors has them attached by pins to the inner cryostat, deliberately allowing a thin layer of Xe to penetrate between the titanium and the PTFE, thus mitigating against alpha particles emitted from U and Th contaminants in dust on the cryostat surface from inducing (α,n) reactions on the adjacent PTFE reflector. Between the inner and outer cryostats is the vacuum region. Dust here has been considered on the titanium surfaces, the MLI superinsulation, which is aluminized mylar, and displacer foam. Beyond the cryostats, there is a layer of displacer foam for mechanical stability, the outer

detector comprised of acrylic vessels holding gadolinium loaded scintillator, mechanical supports, the water tank and its PMTs and reflective liners. While some of these have large areas, our calculations suggest that their distance from the fiducial volume prevent them from posing significant concern under any reasonable assumption of dust level on their surfaces. Dust contributes a negligible 0.19 ER counts to the background in LZ before any discrimination is applied. The total NR contribution from dust is similarly low, at 0.05 counts before application of NR efficiency. These contributions are included in Table 9.2.7.

Detailed cleanliness protocols to clean components and maintain purity are developed for each subsystem, specific to the materials and adopting industry standard cleaning procedures. Each protocol is defined to satisfy the cleanliness goal rather than just the requirement. Each subsystem develops its own cleanliness protocols that are reviewed by the cleanliness working group before being put into effect. The protocols describe how the subsystem components are to be cleaned and kept clean through fabrication, assembly, integration and installation, and describe the validation of cleaning and assay methods. Documentation with each component demonstrates that protocols have been followed step-by-step, and includes results from assay of witness plates and coupons, and from environmental monitoring during fabrication and storage. Upon delivery to SURF each component's documentation pack will include a requirement for signoff for dust cleanliness at the required level. The protocols and documentation are stored in the LZ Information Repository. No part is to be accepted for final assembly and integration on-site without QA and requisite documentation that protocols having been successfully followed.

Final shipping of clean components will involve the use of sealed bags made from films of certified cleanliness. Vendors have been identified for procurement of 50 micron thick Nylon bags certified to be dust free at Level 50 of U.S. MIL-SPEC 1246C, equivalent to there being less than one 50 µm sized particle per square foot. For large components, custom–fabricated bags meeting cleanliness requirements will be used. The standard packaging procedure will employ three layers of packaging: outermost will be "bug bag" which will be removed just before transferring the package from the loading dock to an inside climate–controlled area; the next layer of packaging will be removed in an anteroom to the cleanroom assembly/integration area; and the innermost package will be removed inside the cleanroom just before the part is integrated. Dust deposition rates of 1 ng/cm^2/h have been achieved previously by the SNO experiment, and by the LZ SDSM&T group.

Essential to evaluating cleanliness is the ability to assay at the required levels to maintain QC and perform QA before components are accepted for integration. Several methods for the assay of dust have been developed for the LZ project. At SDSM&T, an optical system has been used. Glass witness slides are imaged, revealing dust, fibers and hairs that have been deposited onto the slides. An automated software process analyses these images and determines the size and mass of each particle. Sensitivity at the level of 5 ng/cm^2 has been demonstrated, sufficient not only for our requirement but also for our goal. In parallel, tape lifts are also being used on non-transparent surfaces, such as Cirlex that is to be used in the PMT bases. Acetate tape is first immersed in acetone and then placed on the surface of the material to be assayed. The tape secures the dust and, once dry, is removed along with the dust. This tape is then optically imaged using the same method as for the glass witness slides. The size distributions for all surfaces assayed broadly follows the expected logarithmic behavior, with the majority of particles measuring below 10 µm and only a few larger. However, these few larger particles dominate the mass of the sample. For large areas of titanium sweeping of dust from the surface and then measurement of the weight of that material is possible with sensitive scales. An area of 1 m^2 with dust deposition at the level of 5 ng/cm^2 equates to a mass of 50 µg, an amount that may be collected and measured with a standard microbalance.

9.6.2 Radon Plate–out

Radon plate-out is a phenomenon in which charged radon progeny are deposited onto the surfaces of materials exposed to air that typically contains concentrations of ^{222}Rn ($T_{1/2}$ =3.82 d) ranging from tens to hundreds of

Bq/m^3 [36, 37]. The decay daughters can be embedded into material as they recoil due to subsequent decays. Beyond radon concentration and surface area, the susceptibility to plate-out depends on the material and factors such as air-flow rates, which are difficult to predict and therefore must be measured. In the cases where measurements are not available, conservative estimates are used to predict contamination risk from plate-out. Plate-out may be further enhanced in the presence of an electric field, since positively charged radon daughters are deposited on negatively charged surfaces such as electrodes within the TPC. The background due to radon daughters on the surfaces arises predominantly from neutron production. In particular the long-lived ^{210}Pb ($T_{1/2}$ =22.3 y) in the decay series decays to ^{210}Po (via ^{210}Bi), which emits an α that feeds (α,n) reactions. In addition to neutron background, progeny from Rn plated onto the inner surfaces of the TPC, particularly ^{206}Pb, can lead to spatial leakage of mis-reconstructed events at the TPC walls, rapidly reducing the fiducial mass. Furthermore, incomplete charge collection of these recoils at the edges of the TPC can cause them to overlap with the low-energy NR band. We have conducted detailed simulations, utilizing the position reconstruction algorithm successfully deployed in both LUX and ZEPLIN-III and adapted for the TPC, extraction electrodes, and top PMT array configurations of LZ, to study position reconstruction of such edge events. In the following we describe in detail our estimate of the level of background produced by plate–out, our approach to estimating the rate at which plate–out could occur in LZ, and the measures we will take to adequately mitigate background risk.

The first background due to (α,n) depends on the area and material composition of component surfaces. It also depends on the degree of surface contact between two components. As described for α's from dust above, if two components are in close contact, α's emitted from the surface of one material could induce (α,n) in the other material. Of the LZ detector components, the only ones with a significant product of surface area and (α,n) reaction yield are the teflon components, due to the fluorine, and the 10 to 20 layers of superinsulation containing aluminum between the inner and outer vessels of the cryostat. Using results on the simulation of the detector response to neutrons and application of analysis cuts, the expected NR background counts from the (α,n) reaction on teflon and aluminum has been estimated, not only for plate–out activity directly on these surfaces but also for plate-out activity on surfaces of other components (e.g. PMTs) in tight contact with teflon or aluminum. The results are shown in Table 9.6.1, with a low total of only 0.05 NR counts before NR efficiency is applied. This is based on a required surface activity density of 10 mBq/m^2.

The second background is the mis–identification of ion daughters which recoil into the TPC active volume from the decays of radon progeny on the surface of the teflon cylindrical reflectors. In the long–lived ^{210}Pb sub–chain, the only decay capable of producing an ion recoil of sufficient energy is the ^{210}Po decay into an alpha and ^{206}Pb ion. Using a fiducial volume enclosing 5.6 tonne on LXe, the probability that an ion recoil is mis-identified as an NR event has been estimated to be 10^{-6}. At the minimum ^{210}Po activity LZ expects to be able to detect, namely, 0.5 mBq/m^2, the expected NR background is 0.16 counts. This background is expected to be mitigated with straightforward measures since it affects only small S2 signals, and its rate falls as a steep function of the distance of the fiducial volume boundary from the physical reflector surface. It therefore does not affect the peak sensitivity of LZ, and may in any case be removed efficiently through fiducialization. Nonetheless, we include this background in Table 9.2.7, and derive a requirement on plate–out activity on the inside of the TPC walls at 0.5 mBq/m^2.

Radon plate-out may also generate ER background if the ^{210}Pb or any of its daughters become mobile and detach from surfaces to enter the fiducial volume. ^{210}Bi in particular would generate single site ER background if present in the target. As discussed in Section 9.2.2, LUX data has been assessed to place upper limits on the mobility of ^{210}Pb daughters from the TPC walls. For an activity of 0.5 mBq/m^2 on the PTFE panels of the TPC in LZ, an upper limit of 40 ER counts may be expected; a contribution similar to the fixed radioactivity or intrinsic contamination goals.

Table 9.6.1: Expected NR background due to (α,n) reaction from plate–out activity at the level of 10 mBq/m^2.

Component	NR Background
TPC PMTs (3–inch)	0.002
Teflon	0.021
PMT cables (teflon jacket)	0.017
Field-shaping rings	0.004
Superinsulation	0.007
Total	0.051

For evaluating measures to control backgrounds due to plate-out, one must estimate the rate at which plate-out occurs. As already mentioned, plate-out is a complex process depending not only on the concentration of radon in the air and the area of exposed surfaces but also on environmental conditions and surface properties and conditions. We have developed three rate calculators, one ("Guiseppe") that parameterizes the daughter deposition rate in terms of the radon concentration in air, surface area, and a "deposition velocity" that has been measured for different radon daughters under different conditions [36]; a second ("Borexino") based on a model used by the Borexino experiment [38] that parameterizes the daughter deposition rate in terms of radon concentration, a column height (e.g. the height of a cleanroom above a work surface), and plate-out fraction; and a third ("dead–air") based on a pessimistic model in which all of the radon decays in a defined volume result in ^{210}Pb daughters deposited on the enclosing surface of the volume. Plate-out measurements carried out within the LZ collaboration to validate this model under conditions in which radon-laden air was circulated very slowly (one volume exchange every 12 hours) over aluminum, teflon, and glass plates set at the bottom of a 8-liter rectangular purge box gave results consistent with the dead–air model.

Numerical results for the estimated exposure time required for ^{210}Pb activity to reach a level of 10 mBq/m^2 are presented in Table 9.6.2. For the first calculator, the largest measured value for the deposition velocity was used as a conservative value, corresponding to the measured plate-out of ^{218}Po on acrylic; for the second calculator a column height of 2.5 m and a plate-out fraction of 0.01 was used, compatible with radon daughter plate-out onto nylon as measured by Borexino; for the third calculator, the area of the enclosing surface was set to 8.0 m^2 and the volume was set to 3.5 m^3, corresponding approximately to the volume of the TPC.

The estimates from the Guiseppe and Borexino models, in qualitative agreement with each other, indicate that detector fabrication and assembly in well-ventilated areas significantly reduces the plate-out rate. Even with good ventilation, however, the allowed exposure times under typical laboratory conditions (Rn

Table 9.6.2: Allowable exposure times (days) to reach radon daughter plate-out requirements

Maximum Activity (mBq/m^2)	Radon Concentration (Bq/m^3)	Guiseppe	Borexino	Dead-Air
10	20	235	168	13.4
10	0.3	15700	11200	895
0.5	20	11.8	8.4	0.7
0.5	0.3	783	560	44.8

concentration on the level of 20 Bq/m^3) are short for a maximum surface activity of 0.5 mBq/m^2 allowed for the TPC cylindrical reflectors. To assure that radon plate-out is controlled during fabrication, assembly, and integration, the following measures will be taken:

1. Final assembly and integration at SURF of the inner cryostat vessel and all interior components, projected to take approximately 6 months, will be carried out in radon-scrubbed clean room with a design radon concentration of 0.3 Bq/m^3. This dramatically increases the acceptable exposure for the TPC reflectors to meet installation and integration timescales, as shown in Table 9.6.2.

2. During storage and transport, parts will be sealed in at least three layers of nylon or metalized mylar bags backfilled with nitrogen or argon. Metallized mylar and nylon are known to be excellent radon barriers although use of nylon in high-humidity environments significantly degrades its effectiveness. Tests within the LZ collaboration using commercially-supplied 2-mil nylon bags and 2.5-mil aluminized mylar bags have shown that the radon concentration reached inside a single bag after one month is at least two orders of magnitude below external levels in the case of nylon and at least three orders of magnitude less for the case of aluminized mylar.

3. In the case of critical parts for which the storage time is long compared to a month, nitrogen purge boxes will be used.

4. Assembly and integration procedures for the TPC cylindrical reflectors will assure good ventilation to avoid higher plate-out rates which would be expected to occur in a dead-air environment.

5. Witness plates and coupons will be assayed at critical points to assure that plate-out is being controlled at the required level.

6. The detailed prescription for implementing the above measures and documenting that they have been successfully followed will be incorporated into the cleanliness protocol for each subsystem.

Within LZ, two sensitive detectors will be used to carry out the assays to determine surface activity and plate-out. The first is the commercial XIA Ultralow 1800 surface alpha detector system, suitable for routine screening of small samples including our witness plates and coupons. Recently installed and commissioned at Brown University, the detector has already achieved a sensitivity to ^{210}Po at the level of 1 mBq/m^2, easily meeting the requirements for the materials contributing to the (α,n) backgrounds. Based on the experience of operating this instrument at other experiments, we expect to ultimately achieve a sensitivity below 0.5 mBq/m^2 that will match requirements for assaying the inner reflector panels of the TPC to determine an upper limit on ion recoil mis-reconstruction backgrounds. The second detector has been developed by the LZ group at SDSM&T, deploying a panel of large-area Si detectors installed in a large vacuum chamber. This detector allows assays of bulky detector components as well as planar witness plates and coupons. With a single Si detector, a sensitivity to ^{210}Po surface activity at the level of a few mBq/m^2 has already been achieved, meeting requirements for the materials generating (α,n) backgrounds. The full system will be online for routine LZ assays by early-2017. For materials such as Teflon, which are produced in granular form before being sintered in molds, plate-out comprises an additional dimension of risk because surface contamination of the granular form becomes contamination in bulk when the granules are poured into molds. Measurements of ^{210}Pb / ^{210}Po in bulk PTFE to the required sensitivity of 10 mBq/kg will be performed using the Lumpsey detector as previously described in Section 9.4.1.2. At this activity, the ^{210}Pb in the bulk PTFE will contribute a background of 0.1 NR counts and is included in Tab. 9.2.7.

9.7 Liquid Xenon Contamination

Krypton and argon present in the xenon will generate backgrounds that, as with radon emanation, cannot be self-shielded against. Here we outline the strategies for limiting the total background contribution from these elements to a relatively low level of less than 1 µdru total activity from both, equivalent to the ER background from material radioactivity.

9.7.1 Krypton

Krypton contamination dispersed throughout the fiducial volume can generate ER background. ^{85}Kr is a beta-emitter with a half-life of 10.8 y and a dominant (99.6 % branching ratio) bare beta decay mode of endpoint energy 687 keV. Its presence in the atmosphere is largely anthropogenic, resulting from nuclear fuel reprocessing and testing of nuclear weapons [39, 40]. Coupled with a long half-life and diffusion properties as a noble gas, it can become a significant contaminant in the course of the production and storage of Xe.

The isotopic abundance of ^{85}Kr in air is nominally $\sim 2 \times 10^{-11}$ [40, 41]. It is present in some air samples at levels that are 10 % to 20 % higher than this. The XMASS experiment found the ^{85}Kr isotopic abundance in its distilled xenon to be $(0.6 \pm 0.2) \times 10^{-11}$ [42]. For the purpose of calculating the LZ requirement we use an abundance of 2×10^{-11}.

The research-grade Xe used in LUX contained an average 130 ppb ^{nat}Kr/Xe upon procurement and was reduced to (3.5 ± 1.0) ppt in LUX, resulting in a measured event rate of (0.17 ± 0.10) mdru [10]. Recent measurements of the ^{nat}Kr content of the first 100,000 liters of Xe purchased for LZ from Praxair found an average concentration of 1.2 ppb.

The allowed ^{nat}Kr concentration in LZ is determined by requiring that ER backgrounds from ^{85}Kr contribute no more than 10 % of the solar pp neutrino rate. To achieve this, the ^{nat}Kr concentration in the LXe must be less than 0.015 ppt, accounting for the ^{85}Kr isotopic abundance and the beta decay spectrum and branching ratio. This concentration will be accomplished with chromatographic separation at SLAC prior to physics operations (see Section 6.3), followed by a comprehensive program to limit the ingress of air from leaks during storage (see Section 6.2.1). Additional requirements are placed on the acceptable leak rate of the Xe handling system during operations (see Section 6.4), and on the acceptable level of Kr outgassing from detector components (see Chapter 9 of Ref. [43]). There is a corollary requirement of 0.015 ppt ^{nat}Kr detection sensitivity to confirm that the removal and storage programs have been successful (see Section 6.7.)

^{nat}Kr concentration levels of <0.2 ppt have been demonstrated during the LUX production run by double-processing a 50 kg LXe batch.

9.7.2 Argon

Trace quantities of argon are also a concern due to beta-emitting ^{39}Ar, with a 269 y half-life, a 565 keV endpoint energy, and a 100 % branching fraction to the ground state. The isotopic abundance is 8×10^{-16} [44]. This background is constrained to be less than 10 % of ^{85}Kr, resulting in a specification of 4.5×10^{-10} g/g or 2.6 µBq. The Kr removal system, which also removes Ar, should easily achieve this goal.

^{37}Ar is another isotope of concern. It decays via electron capture, producing bare x-rays and Auger electrons between 2 and 3 keV with a 90 % branching ratio. Its half-life is 35 days, similar to ^{127}Xe, but since it is not cosmogenically produced while the Xe is in storage, it is not expected to be present in Xe stockpile at the start of physics operations. Its concentration in air is typically 1.2 mBq/m^3 [45], and at this level it is of secondary importance to the leak rate tolerance of the experiment compared to ^{85}Kr (see Section 6.4). However its local concentration in air may be elevated depending on soil conditions, being produced via neutron capture on calcium. We are pursuing a measurement of the ^{37}Ar activity of the Davis campus air in

collaboration with the Pacific Northwest National Laboratory to confirm that it is not a driving factor for the leak rate tolerance of the experiment.

9.8 Laboratory and Cosmogenic Backgrounds

Mitigation of external radioactivity arising from the laboratory environment or from cosmic-ray muons is largely derived from the LZ water shielding and OD. Use of the LXe skin and fiducial volume definition in the TPC for single scatter events also reduces this background, as well as radioactivity arising from cosmogenic activation of materials in the LZ project during manufacture, transport, or storage. Cosmogenic activation of the Xe target also produces radioisotopes but these are intrinsic to the LXe target and cannot be shielded against. While such cosmogenic production of radioisotopes underground in LXe may be neglected due to the low cosmic-ray flux, it is surface activation during production and storage that will generate background in LZ. These backgrounds are shown in Table 9.8.1, and are discussed in the following subsections.

9.8.1 Laboratory Backgrounds

The background in the underground SURF facility outside the water tank is dominated by γ-rays and neutrons produced in the cavern walls. The sources of these γ-rays and neutrons are the uranium and thorium decay chains with a contribution of ^{40}K decay to high-energy γ-rays. Many samples of rock have been screened to get U and Th contamination varying from 0.1 ppm to 7.5 ppm U, from 1.9 ppm to 47 ppm Th and from 0.04 % to 3.3 % of natural potassium, depending on a specific sample and rock formation [46, 47]. At the 4850 level, the γ-ray flux has been measured as (2.16 ± 0.06) /cm^2/s above 0.1 MeV and (0.632 ± 0.019) /cm^2/s above 1 MeV [48]. This agrees well with the simulations of γ-ray flux based on the average values of contamination in the Homestake formation: 1.51 ppm U, 7.38 ppm Th and 0.96 % of natural potassium [48]. Some other sources indicate a lower contamination of U/Th in rock around the lab (down to 0.22 ppm U and 0.33 ppm Th) but the shotcrete and concrete on the walls may give the radioactivity levels an order of magnitude higher and similar to (or even higher than) those quoted above for the Homestake formation (see for instance [49] and references therein). Recently the flux and spectrum of γ-rays in the laboratory hall (East Counting Room) have been measured with a bare HPGe detector [50]. The intensities of γ-ray lines from U, Th and K have been found to be higher than previously reported, giving the integrated flux of 2.19 /cm^2/s for energies >1 MeV with a large uncertainty (about a factor of 2 towards lower flux values) due to the fact that the flux

Table 9.8.1: Events expected from different external or activation sources in 1,000 d live exposure of 5.6 tonne fiducial mass in LZ. Rates are given before expected 99.5 % discrimination for ER events or 50 % efficiency for NRs, with the exception of the last row where the expected count rate in the WIMP search region is quoted.

Source	Recoils	Number of events	Systematic uncertainty
Walls	ER	4.1 ± 0.8	Factor of 2
Walls	NR	<0.001	Included in the limit
Muons	NR	<0.056	30 %
^{127}Xe	ER	0.11	Factor of 5
^{46}Sc	ER	<0.1	Included in the limit
Total	(99.5 % discr., 50 % NR)	0.01 – 0.09	Included in the range

in the continuum comprises Compton scattering events in the detector itself, with no on-site calibration of the detector. Recent measurements of a sample of gravel from beneath the LZ water tank [51] have revealed concentrations of 1.65 ppm U, 0.30 ppm Th and 0.066 % of natural potassium, significantly smaller than previous reports. In our estimates we have used the results from [50] as a conservative estimate.

The γ-ray and neutron fluxes from rock have been shown to be attenuated by many orders of magnitude by the water shielding and then by the LUX background rejection strategy so they do not contribute to the measured number of events in LUX. LZ, however, is expected to achieve 100× better sensitivity to WIMPs and the thickness of shielding is slightly reduced compared to LUX due to a larger cryostat. We have simulated γ-ray production in U and Th decay chains and from ^{40}K, and transport of these γ-rays from lab walls through the shielding down the LXe detector in several steps and applied the same event selection algorithms as for other background sources. The decay chain of Th should give the highest contribution because of the presence of the most energetic 2.62 MeV γ-ray line in the Th decay chain. The simulation results have been normalized to high-energy line intensities as measured in [50] which suggested the concentrations of 6.42 ppm (26.1 Bq/kg) Th, 5.95 ppm U (73.4 Bq/kg) and 2.31 % of natural K (716 Bq/kg of ^{40}K). Our simulations have shown that the number of single ER events in 5.6 tonne of fiducial volume and a live-time of 1,000 d after all cuts is 4.1 ± 0.8 dominated by the 2.6 MeV gammas from Th decay chain. The errors are purely statistical and have been calculated from the number of observed events in simulations. The systematic uncertainty is about a factor of 2. Assuming discrimination power of 99.5 % the limit on the number of events in the NR band will be <0.05 events, much less than the background from internal sources and neutrinos. Neutrons from the laboratory walls are attenuated efficiently by water and scintillator that will surround the LZ cryostat with a minimum thickness of hydrogenous shielding to be 70 cm and a reduction of the neutron flux by more than 6 orders of magnitude. We have carried out simulations of neutron transport through rock and shielding beneath the detector where one of the conduits is located and have shown that no neutrons are likely to pass through this bottom conduit to the LXe target. Other conduits are smaller in diameter and longer which, together with a big thickness of water and scintillator make other sides of the detector better protected against neutrons from rock. This will bring the event rate from rock neutrons to less than 0.001 events in 5.6 tonne fiducial mass for a live time of 1,000 d, well below the contribution from detector components.

Muon-induced neutron production and impact in LZ has been assessed using full Monte Carlo. Muon simulations for LZ were carried out using accurate surface profile for the Davis campus at the 4850 level at SURF. Initially, muons with different energies at the surface were transported through various thicknesses of rock using MUSIC [52, 53]. The resulting spectra of surviving muons have been convolved with muon spectra at the surface for different zenith angles and slant depths. Underground muons have been sampled on the surface of a box which contained the cavern and 5 m to 7 m of rock around the cavern using the MUSUN code [52] and transported through the rock and the detector using LZSim. All particles have been tracked and their interactions in LXe and OD recorded. Selection of surviving events has been based on energy deposition, hit multiplicity, fiducial volume and the anti-coincidence with LXe skin and the Outer Detector; identical to all other event selection criteria in LZSim background simulations. No candidate events has survived the cuts following 118.5 y of equivalent live time. The rejection efficiency of muon-induced neutron background benefits from the large multiplicity of particles produced in cascades initiated by muons. The absence of observed events after cuts allows us to set a 90 % CL upper limit on the muon-induced background rate in LZ of 0.056 NR events for a live-time of 1,000 d, reduced to 0.023 events after applying the 50 % NR efficiency.

9.8.2 Cosmogenic Activation

The irradiation of xenon by cosmic rays at the surface produces a number of radioactive isotopes including those of Xe, tritium, ^{134}Cs, ^{125}I, ^{121m}Te, ^{123m}Te. These cannot be shielded against but non-xenon isotopes

will be efficiently removed from the xenon during purification. Radioisotopes of Xe that can be produced through cosmogenic or neutron activation are ^{127}Xe ($T_{1/2}$ =36.4 d), ^{129m}Xe ($T_{1/2}$ =8.9 d), ^{131m}Xe ($T_{1/2}$ =11.9 d), and ^{133}Xe ($T_{1/2}$ =5.3 d). Most of these will decay quickly and will not pose any threat after a few months of commissioning and calibration runs. Decaying xenon isotopes, in particular ^{131m}Xe, and ^{129m}Xe, will also serve as important calibration sources in these early runs. The exception will be ^{127}Xe, with a half-life of 36.4 d. LUX measurements [10] showed a decay rate of (2.7 ± 0.5) mBq/kg of ^{127}Xe after xenon was exposed to cosmic rays at the Earth's surface. This can be a factor of 3-4 higher if xenon is stored on the surface at SURF (at about 1,600 m elevation).

^{127}Xe produces energy depositions within the WIMP search region of interest and also poses a background for axion searches. ^{127}Xe undergoes electron capture that results in an orbital vacancy that is filled by electron transitions from higher orbitals, resulting in an X-ray or Auger electron cascade. An 85 % probability for the capture electron coming from the K shell results in a cascade with a total energy of 33 keV. A further 12 % of captures from the L shell generate cascades of 5.2 keV total energy deposition, and the remaining 3 % of decays come from higher shells (M and N) to deposit up to 1.2 keV. For a WIMP search energy window of 1.5 keV_{ee} to 6.5 keV_{ee}, significant numbers of L, M, and N shell decays will generate background. However, the daughter ^{127}I nucleus is left in either a 619 keV, 375 keV, or 203 keV excited state (with no direct population of the ground state as part of the electron capture). The subsequent decay of the ^{127}I to the ground state emits internal conversion electrons or γ-rays that permit almost all of the ^{127}Xe background to be rejected by coincidence tagging only those X-ray/Auger events for which the associated γ-rays are not detected contribute to the low-energy ER background in the Xe active region. This effect is expected predominantly at the edge of the Xe target. For example, with a mean free path of 2.6 cm in LXe, the 375 keV γ-ray can potentially escape the active region, reducing the efficiency of coincidence rejection further for events at the edges of the LXe, as seen in LUX [10]. LUX data showed that, after a cooling down period, 0.115 mBq/kg of ^{127}Xe produced a background single hit rate of 0.5×10^{-3} events/keV/kg/d in the ROI. In LZ, the skin and external veto systems significantly aid rejection and characterization of this background. Our simulations with LZSim show that the initial ER background in LZ after cuts at 1.5 keV_{ee} to 6.5 keV_{ee} is 0.22 events per day (assuming no exposure to cosmic rays at 1,600 m elevation). After 8 months of cooling down time underground this rate drops by two orders of magnitude to 0.0022 events/day or about 0.11 events for a live time of 1,000 d (before discrimination and taking into account the continuous decay of the isotope). The early storage of xenon underground mitigates this background further.

The most dangerous isotope due to activation of titanium, used to manufacture the cryostat and many internal detector components, is ^{46}Sc ($T_{1/2}$ = 83.8 d). Using GEANT4 and ACTIVIA [54] codes, we have determined that after 6 months of activation of titanium at sea level, the decay rate of ^{46}Sc will be 2.4 mBq/kg. This is consistent with measurements from LUX [10]. Assembling the TPC within the inner vessel at the surface at SURF will increase this rate by a factor of 2. The beta-decay of ^{46}Sc is almost always followed by the emission of two γ-rays, of energies 1,120 keV and 889 keV. We expect that, after 8 months of cooling, activated ^{46}Sc will contribute less than 0.1 event for a live-time of 1,000 d of LZ operation before 99.5 % discrimination, rendering this background negligible. Effects from activation of other materials are small compared to possible background rates from activated xenon and titanium due to either smaller masses of materials in the vicinity of the LXe target (copper, stainless steel) or absence of long-lived 'dangerous' radioactive isotopes (PTFE). Activation of various materials underground has also been evaluated using GEANT4 and found to be negligible.

9.9 Bibliography

[1] D. S. Leonard *et al.*, Nucl. Instrum. Meth. **A591**, 490 (2008), arXiv:0709.4524 [physics.ins-det].

[2] D. S. Akerib *et al.* (LUX), Nucl. Instrum. Meth. **A704**, 111 (2013), arXiv:1211.3788 [physics.ins-det].

[3] H. M. Araújo *et al.* (ZEPLIN-III), Astropart. Phys. **35**, 495 (2012), arXiv:1104.3538 [physics.ins-det].

[4] E. Aprile *et al.* (XENON100), Phys. Rev. **D83**, 082001 (2011), [Erratum: Phys. Rev. **D85**, 029904 (2012)], arXiv:1101.3866 [astro-ph].

[5] E. Aprile *et al.* (XENON100), J. Phys. **G40**, 115201 (2013), arXiv:1306.2303 [astro-ph].

[6] C. Ghag *et al.* (ZEPLIN-III), Astropart. Phys. **35**, 76 (2011), arXiv:1103.0393 [astro-ph].

[7] N. Abgrall *et al.* (Majorana), Adv. High Energy Phys. **2014**, 365432 (2014), arXiv:1308.1633 [physics.ins-det].

[8] A. Gando *et al.* (KamLAND-Zen), Phys. Rev. **C85**, 045504 (2012), arXiv:1201.4664 [hep-ex].

[9] F. P. An *et al.* (Daya Bay), Phys. Rev. Lett. **112**, 061801 (2014), arXiv:1310.6732 [hep-ex].

[10] D. S. Akerib *et al.* (LUX), Astropart. Phys. **62**, 33 (2015), arXiv:1403.1299 [astro-ph].

[11] S. Agostinelli *et al.* (GEANT4), Nucl. Instrum. Meth. **A506**, 250 (2003).

[12] D. S. Akerib *et al.* (LUX), Nucl. Instrum. Meth. **A675**, 63 (2012), arXiv:1111.2074 [physics.data-an].

[13] M. Szydagis, N. Barry, K. Kazkaz, J. Mock, D. Stolp, M. Sweany, M. Tripathi, S. Uvarov, N. Walsh, and M. Woods (NEST), J. Instrum. **6**, P10002 (2011), arXiv:1106.1613 [physics.ins-det].

[14] E. Aprile *et al.* (XENON100), Astropart. Phys. **35**, 43 (2011), arXiv:1103.5831 [physics.ins-det].

[15] E. Aprile *et al.* (XENON1T), Eur. Phys. J. **C75**, 546 (2015), arXiv:1503.07698 [astro-ph.IM].

[16] J. Boger *et al.* (SNO), Nucl. Instrum. Meth. **A449**, 172 (2000), arXiv:nucl-ex/9910016 [nucl-ex].

[17] D. S. Akerib *et al.* (LUX), Nucl. Instrum. Meth. **A703**, 1 (2013), arXiv:1205.2272 [physics.ins-det].

[18] A. Gando *et al.* (KamLAND-Zen), Phys. Rev. Lett. **117**, 082503 (2016), [Addendum: Phys. Rev. Lett.117,no.10,109903(2016)], arXiv:1605.02889 [hep-ex].

[19] G. Alimonti *et al.* (Borexino), Nucl. Instrum. Meth. **A600**, 568 (2009), arXiv:0806.2400 [physics.ins-det].

[20] D. C. Malling, S. Fiorucci, M. Pangilinan, J. J. Chapman, C. H. Faham, J. R. Verbus, and R. J. Gaitskell, "Dark Matter Search Backgrounds from Primordial Radionuclide Chain Disequilibrium," (2013), (unpublished), arXiv:1305.5183 [astro-ph].

[21] C. Ghag, *Proceedings, 5th Topical Workshop on Low Radioactivity Techniques (LRT 2015): Seattle, WA, USA, March 18-20, 2015*, AIP Conf. Proc. **1672**, 020003 (2015).

[22] D. Yu. Akimov *et al.* (ZEPLIN-III), Astropart. Phys. **34**, 151 (2010), arXiv:1004.4207 [hep-ex].

[23] B. D. LaFerriere, T. C. Maiti, I. J. Arnquist, and E. W. Hoppe, Nucl. Instrum. Meth. **A775**, 93 (2015).

[24] P. Grinberg, S. Willie, and R. Sturgeon, Anal. Chem. **77**, 24322436 (2005).

[25] D. S. Leonard, J. Korean Phys. Soc. **64**, 1878 (2014).

[26] The MIT Nuclear Reactor Laboratory, (2015), 138 Albany Street, Cambridge, MA 02139-4201.

[27] J. Mott, in *Low Radioactivity Techniques 2013 (LRT 2013): Proceedings of the IV International Workshop in Low Radioactivity Techniques*, AIP Conf. Proc., Vol. **1549**, edited by L. Miramonti and L. Pandola (2013) pp. 152–155, *Low-background tracker development for the SuperNEMO experiment*, Conference Presentation.

[28] H. Richter, H. Simgen, and G. Zuzel (GERDA), "^{222}Rn Measurements," (2008), Presented at GERDA Collaboration Meeting: Crakow, Poland, USA, Feb. 18-20, 2008.

[29] S. Lindemann, *Intrinsic ^{85}Kr and ^{222}Rn Backgrounds in the XENON Dark Matter Search*, Ph.D. thesis, University of Heidelberg (2013).

[30] D. Tiedt, *Radioactive Background Simulation and Cleanliness Standards Analysis for the Long Baseline Neutrino Experiment Located located at the Sanford Underground Research Facility*, Master's thesis, South Dakota School of Mines and Technology (2013).

[31] E. D. Hallman and R. G. Stokstad, *Establishing a Cleanliness Program and Specifications for the Sudbury Neutrino Observatory*, Tech. Rep. SNO-STR-91-009 (Sudbury Neutrino Observatory, Department of Physics, Stirling Hall, Queen's University at Kingston, Kingston, Ontario, Canada K7L 3N6, 1991).

[32] D. Parasuraman, A. Kemps, H. Veeke, and G. Lodewijks, J. IEST **55**, 1 (2012).

[33] R. R. Schumann and L. C. Gundersen, Environ. Int. **22**, 439 (1996).

[34] H. W. Lee, *Radon in the Acrylic Vessel*, Tech. Rep. SNO-STR-94-028 (Sudbury Neutrino Observatory, Department of Physics, Stirling Hall, Queen's University at Kingston, Kingston, Ontario, Canada K7L 3N6, 1994).

[35] R. Heaton, H. Lee, P. Skensved, and B. C. Robertson, Nucl. Instrum. Meth. **A276**, 529 (1989).

[36] V. E. Guiseppe, S. R. Elliott, A. Hime, K. Rielage, and S. Westerdale, in *Topical Workshop on Low Radioactivity Techniques: LRT-2010*, AIP Conf. Proc., Vol. **1338**, edited by R. Ford (2011) pp. 95–100, *A Radon Progeny Deposition Model*, Conference Presentation, arXiv:1101.0126 [nucl-ex].

[37] C. Arpesella *et al.* (Borexino), Astropart. Phys. **18**, 1 (2002), arXiv:hep-ex/0109031 [hep-ex].

[38] T. Shutt, (2016), Private Communication.

[39] J. Ahlswede, S. Hebel, J. O. Ross, R. Schoetter, and M. B. Kalinowski, J. Environ. Radioact. **115**, 34 (2013).

[40] P. Collon, W. Kutschera, and Z.-T. Lu, Ann. Rev. Nucl. Part. Sci. **54**, 39 (2004), arXiv:nucl-ex/0402013 [nucl-ex].

[41] X. Du, R. Purtschert, K. Bailey, B. E. Lehmann, R. Lorenzo, Z.-T. Lu, P. Mueller, T. P. O'Connor, N. C. Sturchio, and L. Young, Geophys. Res. Lett. **30**, 2068 (2003).

[42] K. Abe *et al.* (XMASS), Nucl. Instrum. Meth. **A716**, 78 (2013), arXiv:1301.2815 [physics.ins-det].

[43] D. S. Akerib *et al.* (LZ), (2015), Conceptual Design Report; LBNL-190005, FERMILAB-TM-2621-AE-E-PPD, arXiv:1509.02910 [physics.ins-det].

[44] H. H. Loosli, B. E. Lehmann, and W. M. Smethie Jr., in *Environmental Tracers in Subsurface Hydrology*, edited by P. G. Cook and A. L. Herczeg (Springer US, 2000) pp. 379–396, *Noble Gas Radioisotopes: ^{37}Ar, ^{85}Kr, ^{39}Ar, ^{81}Kr*, ISBN 978-1-4613-7057-4.

[45] R. A. Riedmann and R. Purtschert, Environ. Sci. Technol. **45**, 8656 (2011).

[46] K. T. Lesko *et al.*, (2011), DUSEL Preliminary Design Report, p. 3-138, arXiv:1108.0959 [hep-ex].

[47] W. Roggenthen and A. R. Smith, "Uranium, Thorium, Potassium Contents of Materials in the Homestake Underground, Lead SD," (2008), AGU Fall Meeting, San Francisco, CA.

[48] D.-M. Mei, C. Zhang, K. Thomas, and F. Gray, Astropart. Phys. **34**, 33 (2010), arXiv:0912.0211 [nucl-ex].

[49] K. T. Lesko, *Proceedings, 13th International Conference on Topics in Astroparticle and Underground Physics (TAUP 2013): Asilomar, California, September 8-13, 2013*, Phys. Procedia **61**, 542 (2015).

[50] K. J. Thomas (LZ), *An Estimate of the Gamma Flux in the East Counting Room of the Davis Cavern*, Tech. Rep. (Lawrence Berkeley National Laboratory (LBNL), 1 Cyclotron Road, Berkeley, CA 94720-8099, USA, 2014).

[51] D. Harvey, K. Thomas, and A. R. Smith (LZ), *LUX Water Tank Gravel*, Tech. Rep. (Lawrence Berkeley National Laboratory (LBNL), 1 Cyclotron Road, Berkeley, CA 94720-8099, USA, 2016).

[52] V. A. Kudryavtsev, Comput. Phys. Commun. **180**, 339 (2009), (MUSIC), arXiv:0810.4635 [physics.comp-ph].

[53] P. Antonioli, C. Ghetti, E. V. Korolkova, V. A. Kudryavtsev, and G. Sartorelli, Astropart. Phys. **7**, 357 (1997), (MUSIC), arXiv:hep-ph/9705408 [hep-ph].

[54] J. J. Back and Y. A. Ramachers, Nucl. Instrum. Meth. **A586**, 286 (2008), (ACTIVIA), arXiv:0709.3472 [nucl-ex].